

AD-A255 845



RL-TR-92-157
Final Technical Report
June 1992



RESULTS OF THE LASER SENSOR TECHNOLOGY TRANSITION INVESTIGATION

SCITEC, Inc.

Dr. Richard Preston



APPROVED FOR PUBLIC RELEASE; DISTRIBUTION UNLIMITED.

This effort was funded totally by the Laboratory Director's fund.

92 9 28 018

Y23439 **92-25975** *11
pgs*



**Rome Laboratory
Air Force Systems Command
Griffiss Air Force Base, NY 13441-5700**

This report has been reviewed by the Rome Laboratory Public Affairs Office (PA) and is releasable to the National Technical Information Service (NTIS). At NTIS it will be releasable to the general public, including foreign nations.

RL-TR-92-157 has been reviewed and is approved for publication.

APPROVED:



MARK WILBANKS, Capt, USAF
Project Engineer

FOR THE COMMANDER:



THADEUS J. DOMURAT
Technical Director
Intelligence & Reconnaissance Directorate

If your address has changed or if you wish to be removed from the Rome Laboratory mailing list, or if the addressee is no longer employed by your organization, please notify RL (IRAE), Griffiss AFB NY 13441-5700. This will assist us in maintaining a current mailing list.

Do not return copies of this report unless contractual obligations or notices on a specific document require that it be returned.

REPORT DOCUMENTATION PAGE

Form Approved
OMB No. 0704-0188

Public reporting burden for this collection of information is estimated to average 1 hour per response, including the time for reviewing instructions, searching existing data sources, gathering and maintaining the data needed, and completing and reviewing the collection of information. Send comments regarding this burden estimate or any other aspect of this collection of information, including suggestions for reducing this burden, to Washington Headquarters Services, Directorate for Information Operations and Reports, 1215 Jefferson Davis Highway, Suite 1204, Arlington, VA 22202-4302, and to the Office of Management and Budget, Paperwork Reduction Project (0704-0188), Washington, DC 20503.

1. AGENCY USE ONLY (Leave Blank)	2. REPORT DATE	3. REPORT TYPE AND DATES COVERED
	June 1992	Final
4. TITLE AND SUBTITLE		5. FUNDING NUMBERS
RESULTS OF THE LASER SENSOR TECHNOLOGY TRANSITION INVESTIGATION		C - F30602-88-D-0026 Task 47 PE - 61101F PR - LDFP TA - 08 WU - H1
6. AUTHOR(S)		8. PERFORMING ORGANIZATION REPORT NUMBER
Dr. Richard Preston		
7. PERFORMING ORGANIZATION NAME(S) AND ADDRESS(ES)		10. SPONSORING/MONITORING AGENCY REPORT NUMBER
SCITEC, Inc. P.O. Box CN5203 Princeton NJ 08543-5203		RL-TR-92-157
9. SPONSORING/MONITORING AGENCY NAME(S) AND ADDRESS(ES)		12a. DISTRIBUTION/AVAILABILITY STATEMENT
Rome Laboratory (IRAE) Griffiss AFB NY 13441-5700		12b. DISTRIBUTION CODE
Approved for public release; distribution unlimited.		
13. ABSTRACT (Maximum 200 words)		
This report summarizes experiments carried out at Rome Laboratory (RL) under a Laboratory Director Funds (LDF) effort. Experiments were carried out at both SCITEC and RL in conjunction with the Intelligence and Reconnaissance Directorate and the Photonics Center. Experimental results are described regarding the sensitivity and noise characteristics of commercially available mercury cadmium telluride (MCT) detectors and preamps. Also presented are some measurements of potential ways to reject false alarms.		
14. SUBJECT TERMS		15. NUMBER OF PAGES
Intelligence & Reconnaissance, mercury cadmium telluride (MCT)		72
		16. PRICE CODE
17. SECURITY CLASSIFICATION OF REPORT UNCLASSIFIED	18. SECURITY CLASSIFICATION OF THIS PAGE UNCLASSIFIED	19. SECURITY CLASSIFICATION OF ABSTRACT UNCLASSIFIED
		20. LIMITATION OF ABSTRACT U/L

Block 11 (Continued)

P.O. Box 400, Buffalo NY 14225

This effort was funded totally by the Laboratory Director's fund.

Accession For	
NTIS GRA&I	<input checked="" type="checkbox"/>
DTIC TAB	<input type="checkbox"/>
Unannounced	<input type="checkbox"/>
Justification	
By _____	
Distribution/ _____	
Availability Codes:	
Dist	Avail and/or Special
A-1	

DTIC QUALITY INSPECTED 3

EXECUTIVE SUMMARY

This report describes an experimental effort to investigate CO₂ laser detection and false alarm rejection techniques. The measurements were designed to test sensor performance predictions reported in the Laser Sensor Design Study. Experiments were carried out at both SciTec and the Photonics Laboratory under Lab Director Funds sponsorship. Three principal experiments were involved:

- 1) detector/preamp performance tests including pulse attenuation and noise measurements,
- 2) cosmic ray and electronic noise responses of a variety of detector types and materials,
- 3) CO₂ gas cell differential absorption measurements for a possible false alarm rejection technique.

Experiments were carried out using equipment borrowed from a variety of sources including SciTec, RL, DIA, WL, CNVEO. The principal findings of the effort are summarized below.

Detector/Preamp Performance Tests

Three different preamps were designed for use with a 0.25 mm photovoltaic mercury-cadmium-telluride (MCT-PV) detector. The preamps were designed with bandwidths of 3.5 MHz, 350 kHz, and 35 kHz to measure 0.1, 1.0, and 10 microsecond pulses, respectively. Pulse attenuation measurements by the detector/preamps were reasonably predicted by a single pole RC filter model for the appropriate bandwidths. However, since the polygon scanner was not able to create 10 microsecond pulses, a new technique, perhaps using a single hole chopper, needs to be devised for future tests.

RMS noise measurements with the wide band amplifier were approximately twice the predicted values and the noise spectrum revealed considerable peaking at 400 kHz. A similar feature at 460 kHz dominated the 350 kHz amplifier's noise spectrum and its RMS noise voltage was over an order of magnitude higher than predicted. The 350 kHz amplifier produced a noise value close to the predicted one when connected to a detector simulator circuit which mimicked the vendor's reported electrical characteristics for the detector. Evidently, the detector has other characteristics, not represented by standard photovoltaic detector models, which interact with the circuit in a way to create oscillations. Both of the wider bandwidth amplifiers use the same op amp in their circuits and we recommend discussing the problem with the amplifier vendor in a future effort.

The 35 kHz amplifier was lacking a principal noise spectral feature as seen in the other bandwidth amplifiers. However, its rms noise value was still over an order of magnitude higher than predicted. None of the three amplifiers' rms noise levels were affected by the background incident on the detector, even up to a 1000°C blackbody background.

Overcoming the noise problems for the MCT receivers will be critical for their use in the RL scenarios currently defined. The strong spectral features in the wider band amplifiers can probably be overcome straightforwardly. However, discussions with detector vendors and other

experts (e.g., Professor Derniak at the University of Arizona) are warranted in a future effort to understand the lower bandwidth amplifier's noise problem.

Cosmic Ray Experiment

Threshold crossing events for various detectors were captured on a digital oscilloscope and downloaded to a computer for analysis. MCT-PV, photoconductive MCT (MCT-PC), silicon, and silicon-avalanche photodiode detectors were all tested. Cosmic ray events were distinguishable from spurious noise glitches because of their consistent pulse shape corresponding to the system's impulse response. Noise pulses from outside sources (e.g., power line glitches) were highly oscillatory in nature. For the lower bandwidth amplifiers, threshold crossings were also seen with durations much shorter than the system response time.

Cosmic ray rates were estimated from the threshold crossing data by subtracting out the non-cosmic ray events and dividing by the sample time and detector area. Calculated rates varied widely depending on the period sampled, the detector material, and the signal bandwidth. Additional analysis on the pulselwidth and pulse amplitude distributions of the cosmic ray data is needed in a future effort. The cosmic ray rate for the MCT-PV detector appeared anomalously high possibly due to a common anode connection between the detector we used and eight other detectors in the dewar. If this turns out to be the case, it has important implications for future sensor designs using array detectors as recommended in the RL sensor study. Measurements of the cosmic ray rates from different area detectors in the same dewar would test this hypothesis. If there is no area dependence to the cosmic ray rate, then there is a cross-talk problem with the detectors.

Gas Cell Absorption Experiment

Tests with the CO₂ gas cell validated the CO₂ laser absorption coefficients predicted by FASCODE. The 1000°C blackbody transmission measurements did not agree as well as the laser case, although the discrepancy may be attributable to the experimental technique. Broadband transmission measurements with a pulsed radiation source are needed to validate the predictions. Nevertheless, the technique appears to be a useful false alarm discriminant for CO₂ lasers. Outdoor tests with false alarm sources at longer ranges are needed to test the technique in a non-laboratory environment. We recommend building a breadboard receiver using the CO₂ absorption cell technique.

ACKNOWLEDGEMENTS

The author gratefully acknowledges the support of Captain Mark Wilbanks and Rome Laboratory Intelligence and Reconnaissance Directorate for their financial support and technical encouragement throughout the effort. For laboratory space, equipment loans, and personnel support, the author thanks the Photonics Center. In particular, the experimental help of John Malowicki, Jim Theinar, and Paul Reepak are noted. Mr. Bill Kaveney's moral support was also appreciated.

The author also would like to thank: Captain Vivian Wolf and Mrs. Barbara Sanderson of DIA for the use of their AOTF radiometer; Matt Dierkin and Jack Parker of Wright Laboratories for loaning us an RF power supply; Wayne Antesburger and Mark Norton of the Center for Night Vision and Electro-Optics for use of a laser detection sensor, and Bob Ghormley of the Community Laser Measurement Program (C-LAMP) at Sandia National Laboratory, Albuquerque, for use of the Redbird radiometers.

TABLE OF CONTENTS

	<u>Page</u>
ABSTRACT	ii
EXECUTIVE SUMMARY	iii
ACKNOWLEDGEMENTS	v
TABLE OF CONTENTS	vi
LIST OF FIGURES	vii
LIST OF TABLES	viii
1. INTRODUCTION	1
2. DETECTOR SENSITIVITY EXPERIMENT	2
2.1 Objectives	2
2.2 Other Agency Sensors Tested	2
2.3 Preamp Designs for MCT-PV Detector	7
2.4 Experimental Approach	7
2.5 Measurement Results and Conclusions	9
2.5.1 Pulse Attenuation Measurements	9
2.5.2 Noise Measurements	9
2.5.3 CNVEO System Sensitivity	21
2.6 Conclusions	21
3. COSMIC RAY DETECTION EXPERIMENT	22
3.1 Objectives and Approach	22
3.2 Experimental Results	22
3.3 Conclusions	32
4. GAS CELL ABSORPTION EXPERIMENT	50
4.1 Theory and Objectives	50
4.2 Experimental Approach	50
4.3 Measurement Results and Conclusions	50
APPENDIX	
Circuit Schematics	55
REFERENCES	59

LIST OF FIGURES

<u>Figure</u>	<u>Page</u>
2-1 Pulse Attenuation Predictions	4
2-2 Polygon Scanner Layout	8
2-3 Noise Spectrum of 3.5 MHz Amplifier and 0.25 mm Detector	15
2-4 Noise Spectrum of 350 kHz Amplifier and 0.25 mm Detector	16
2-5 Frequency Spectra of 350 kHz Amplifier and Detector Simulator	17
2-6 Noise Spectrum for 35 kHz Amplifier and Detector Simulator	19
2-7 Noise Spectrum for 35 kHz Amplifier and 0.25 mm Detector	20
3-1 Cosmic Ray Response of NERC MCT-PV Sensor	25
3-2 Noise Glitch on NERC MCT-PV	26
3-3a NERC Amplifier Response to Noise Glitches	27
3-3b NERC Amplifier Response to Noise Glitches	28
3-4a Noise Pulse Measurements with NERC Detector and 100 MHz Amplifier	29
3-4b Noise Pulse Measurements with NERC Detector and 100 MHz Amplifier	30
3-4c Noise Pulse Measurements with NERC Detector and 100 MHz Amplifier	31
3-5a 20 MHz Silicon APD Noise Results	33
3-5b 20 MHz Silicon APD Noise Results	34
3-5c 20 MHz Silicon APD Noise Results	35
3-6a 0.5 MHz Silicon APD Noise Results	36
3-6b 0.5 MHz Silicon APD Noise Results	37
3-7a 10 kHz Silicon Pin Diode Noise Results	38
3-7b 10 kHz Silicon Pin Diode Noise Results	39
3-7c 10 kHz Silicon Pin Diode Noise Results	40
3-7d 10 kHz Silicon Pin Diode Noise Results	41
3-8a 80 kHz Photo Conductive MCT Results	42
3-8b 80 kHz Photo Conductive MCT Results	43
3-8c 80 kHz Photo Conductive MCT Results	44
3-8d 80 kHz Photo Conductive MCT Results	45
3-8e 80 kHz Photo Conductive MCT Results	46
3-8f 80 kHz Photo Conductive MCT Results	47
4-1 CO ₂ Absorption Spectrum	51
4-2 Experimental Set-Up	52

LIST OF TABLES

<u>Table</u>	<u>Page</u>
1-1 Equipment List	2
2-1 Sensitivity Analysis for 0.5 mm Photovoltaic MCT Detector	5
2-2 Sensitivity Analysis for 0.25 mm Photovoltaic MCT Detector	6
2-3 Measured Pulsewidths for Polygon Scanner	10
2-4 Short Pulse Measurement Results	11
2-5 One Microsecond Pulse Measurement Results	12
2-6 Measured RMS Noise Currents	13
2-7 Sine Wave Response of 350 kHz Amplifier	18
3-1 Detector Characteristics	23
3-2 Summary of Cosmic Ray Runs	24
3-3 Detector Hit Rates	48
4-1 Summary of the Predicted and Measured Experimental Results for the Gas Cell Absorption Experiment	53

1. INTRODUCTION

Approaches for detecting and unambiguously identifying laser radiation are needed for a variety of tactical and intelligence applications. For CO₂ detection sensors, an approach which maintains high sensitivity and good false alarm rejection is needed. In a report⁽¹⁾ for the Intelligence and Reconnaissance Branch of Rome Laboratories (RL), sensitivity estimates were made for several CO₂ detection sensor designs. The purpose of this effort was to begin experimental investigations at RL of actual detector sensitivities and potential false alarm rejection techniques.

The approach taken for this effort was to use proven experimental procedures to characterize existing sensors from a variety of laboratories. Also, some preamplifiers were breadboarded for use with a photovoltaic mercury-cadmium-telluride detector (MCT-pv) to compare measured and predicted pulse attenuation and noise characteristics. Detectors and measurement equipment was contributed by a number of organizations as summarized in Table 1-1. A separate chapter has been written for each experiment carried out under this effort since their objectives, approach, results, and conclusions were distinct. The final chapter is a summary of conclusions with recommendations made regarding directions for further RL laser sensor efforts.

TABLE 1-1. Equipment List

Item	Owner	Purpose
CO ₂ Laser and Chiller	SciTec	Laser radiation source
Blackbody	SciTec	Broadband radiation source and calibration reference
NERC MCT-PV Detector	SciTec	Detector for sensitivity measurements
Chopper	SciTec	Source modulator
Polygon Scanner	SciTec	Creates constant amplitude, variable width pulses from CW laser
CO ₂ Absorption Cell	SciTec	Gas cell for differential absorption measurements
High Speed Digital Oscilloscope and Computer	SciTec	Captures pulse amplitude and pulselength of cosmic rays and downloads them to computer for analysis
AOTF Radiometer	DIA	9-11 micron AOTF, MCT-PC detector associated optics and electronics
RF Power Supply and Amplifier	NADC	Marconi device with fixed center frequency FM capability
Programmable RF Power Supply	WL	Wiltron device with FM and sweep capability
Redbird Sensors	Sandia	MCT-PC detectors used on Sweetwater
CO ₂ Detection Sensor	CNVEO	High sensitivity receiver for comparison with other detectors
Spectrum Analyzer	RL	Characterize noise power spectral density
Oscilloscopes and Miscellaneous Lab Equipment	RL	General experimental support

2. DETECTOR SENSITIVITY EXPERIMENT

2.1 Objectives

The objective of this experiment was to test the sensitivity achieved by different detector types and preamp designs. Photovoltaic and photoconductive MCT were the candidates of interest in this experiment. The approach taken was to design three preamps for different pulsedwidth measurements and compare the predicted and measured preamp performance. Also, several other sensors were borrowed from government agencies to characterize their performance.

2.2 Preamp Designs for MCT-PV Detector

Three special preamps were designed under this effort by Zuchor, Ltd. for a SciTec-owned, 0.25 mm (square), MCT-pv detector from New England Research Corporation (NERC). The designs were 35 kHz, 350 kHz, and 3.5 MHz for measuring 10 microsecond, 1 microsecond, and 0.1 microsecond pulses, respectively. The schematics for the preamps and post-amps and parts descriptions for commercial components are given in Appendix 1. Preamp pulse attenuation predictions for these bandwidths are shown in Figure 2-1.

One of the questions addressed in the amplifier design and testing was whether a sensor could employ a common amplifier with switch selectable gain settings to optimize its performance for particular pulsedwidths. We have concluded that this approach would be a mistake since the best amplifier designs for each bandwidth turned out to be considerably different. Consequently, there are two approaches we recommend to designing array detector systems. The first is to use a modular system approach with detector packages optimized for particular source pulsedwidths. The second is to have most of the detectors in the array be an intermediate bandwidth with several faster and several slower detectors included in the array. If a particular type of pulse is detected repetitively, the sensor pointing could be adjusted to align the detector with the optimal bandwidth on the radiation source.

Table 2-1 presents noise current predictions for a 0.5 mm detector. Table 2-1 is similar to one in the RL Laser Sensor Study final report, although several erroneous noise entries have been corrected. Specifically, the commercial preamplifier's noise was found to be significantly higher than implied by their data sheet. Discussions with the vendor revealed the discrepancy. Despite the higher noise, it is still expected that the 35 kHz system should be background limited. For the 350 kHz system, the background noise contribution should be noticeable.

The preamp noise predictions for a 3.5 MHz system with a 0.25 mm detector are shown in Table 2-2. These predictions are made to match the small MCT detector available for this experiment.

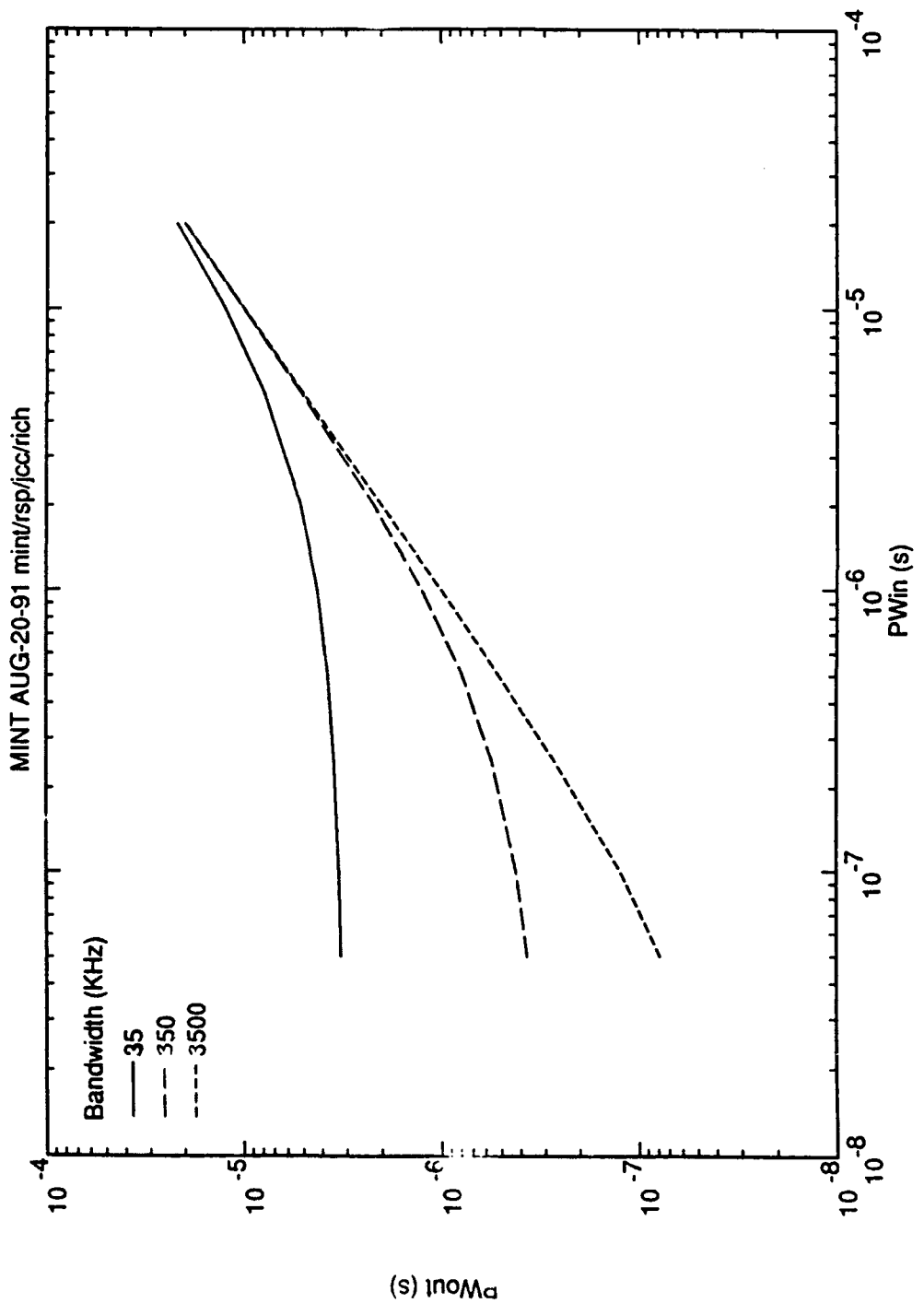


FIGURE 2-1. Pulse Attenuation Predictions

TABLE 2-1. Sensitivity Analysis for 0.5 mm Photovoltaic MCT Detector

$C_{\text{det}}=125 \text{ pF}$, $r_{\text{det}}=200 \text{ ohms}$, $C_{\text{out}}=135 \text{ pF}$

Preamp Components		Current Noise						Performance Estimates		
Rf Ohms	Cf	Detector/Preamp Bandwidth	Due to r_{det}	Due to en_A	Due to R_t	Equiv. i_{in}	Due to BKG Shot Noise in Slitless Spectrometer (Imager)	Total Noise for Slitless Spectrometer (Imager)	NEP for Slitless Spectrometer (Imager)	NEI for Slitless Spectrometer (Imager)
1.5k	.27 pF	3.5 MHz	3.6 nA	18 nA	2.4 nA	6.2 nA	19.2 nA (2.6 nA)	1.7 nA (6.9 nA)	6.6 nA (1.4 nA)	4.8x10 ⁻¹¹ (5.2x10 ⁻¹¹)
550k	.9 pF	350 KHz	115 pA	240 pA	750 pA	170 pA	806 pA (0.84 nA)	0.53 nA (0.86 nA)	0.57 nA (0.17 nW)	4.1x10 ⁻¹² (6.3x10 ⁻¹²)
10M	.5 pF	35 KHz	3.6 pA	16.8 pA	18.4 pA	7.5 pA	18.5 pA (260 pA)	170 pA (260 pA)	171 pA (5.2x10 ⁻¹¹)	3.4x10 ⁻¹¹ (1.9x10 ⁻¹²)

TABLE 2-2. Sensitivity Analysis for 0.25 mm Photovoltaic MCT Detector

$C_{\text{par}}=35 \text{ pF}$, $r_{\text{par}}=800 \text{ ohms}$, $C_{\text{load}}=45 \text{ pF}$

Rf	Cf	Detector/ Preamp Bandwidth	Due to r_{par}	Due to i_{in}	Due to R_i	Equiv. i_s in	BKG Noise FWHM=0.25 Microns	Total Noise
4.99k	8 pF	3.5 MHz	1.8 nA	6 nA	2.4 nA	3.4 nA	7.3 nA	1.0 nA

2.3 Other Sensors Tested

A Center for Night Vision and Electro-Optics (CNVEO) laser detection system was borrowed to characterize its sensitivity. The sensor used two 3-element detector arrays with co-aligned fields-of-view for coincidence detection. The three detector elements were "ored" together to indicate when any one of them crossed threshold. Although the sensor was not designed as a radiometer, its preamp outputs could be accessed on a connector exposed by removing the front cover. Signals measured at the preamp were very poor from a radiometric standpoint, since they oscillated dramatically after crossing threshold. Also, it was difficult to always correlate threshold crossings detected on the preamp with logical indications from the sensor. In one instance, an apparently large signal detected on one preamp did not result in a threshold crossing being exhibited by the indicator light. Therefore, for our sensitivity experiment, we used the flashing light indicator to determine when the sensor's threshold was being exceeded rather than the preamp signal.

Sandia's Redbird radiometer, which was used on the Sweetwater test, was borrowed to measure its pulse attenuation of 1-microsecond pulses. Sandia operated a 1-microsecond pulselength, CO₂ laser as one of the Sweetwater test sources. The Redbird's radiometric signals need to be calibrated so that their data can be used for propagation model validation.

DIA provided an AOTF radiometer for pulse attenuation measurements and frequency modulation tests (see Reference 2). This instrument uses a thallium arsenic selenide (TASS) crystal to diffract light in the 9-11 micron bandpass. A Marconi RF synthesizer and amplifier drives the TASS crystal with RF power in the 15-20 MHz region. Wright Laboratories provided a Wiltron RF synthesizer which provided an FM and sweep capability.

2.4 Experimental Approach

All of the pulse detection sensors were tested using SciTec's polygon scanner, illustrated in Figure 1. The instrument uses a CW laser (CO₂ in this case) to create variable width, constant amplitude pulses. It does this by scanning the beam with a fast, ten-sided mirror which reflects the beam back onto adjacent mirror facets for nine bounces off the mirror. The swept beam is passed across an adjustable slit to create a pulsed radiation source. By adjusting the mirror speed, one can vary the pulselength without changing the amplitude. The pulse amplitude is determined by the beam spot size, the slit width, and the beam intensity. Pulselengths created by the scanner for these experiments ranged from 60 ns to 1 microsecond. The 1-microsecond pulselength was achieved by changing the system's optics so only one mirror bounce occurred. Slower pulselengths could not be achieved without modification to the drive motor.

Pulse attenuation measurements were made with a 2-step procedure. First, the mirror position was fixed so that it steered the CW beam through the slit. With the intensity maximized, the beam was chopped at 1-3 kHz to measure the sensor's response without electronic bandwidth attenuation. Next, the mirror was spun to create the desired pulselength and the attenuated response was measured. Pulselengths created by the scanner were characterized

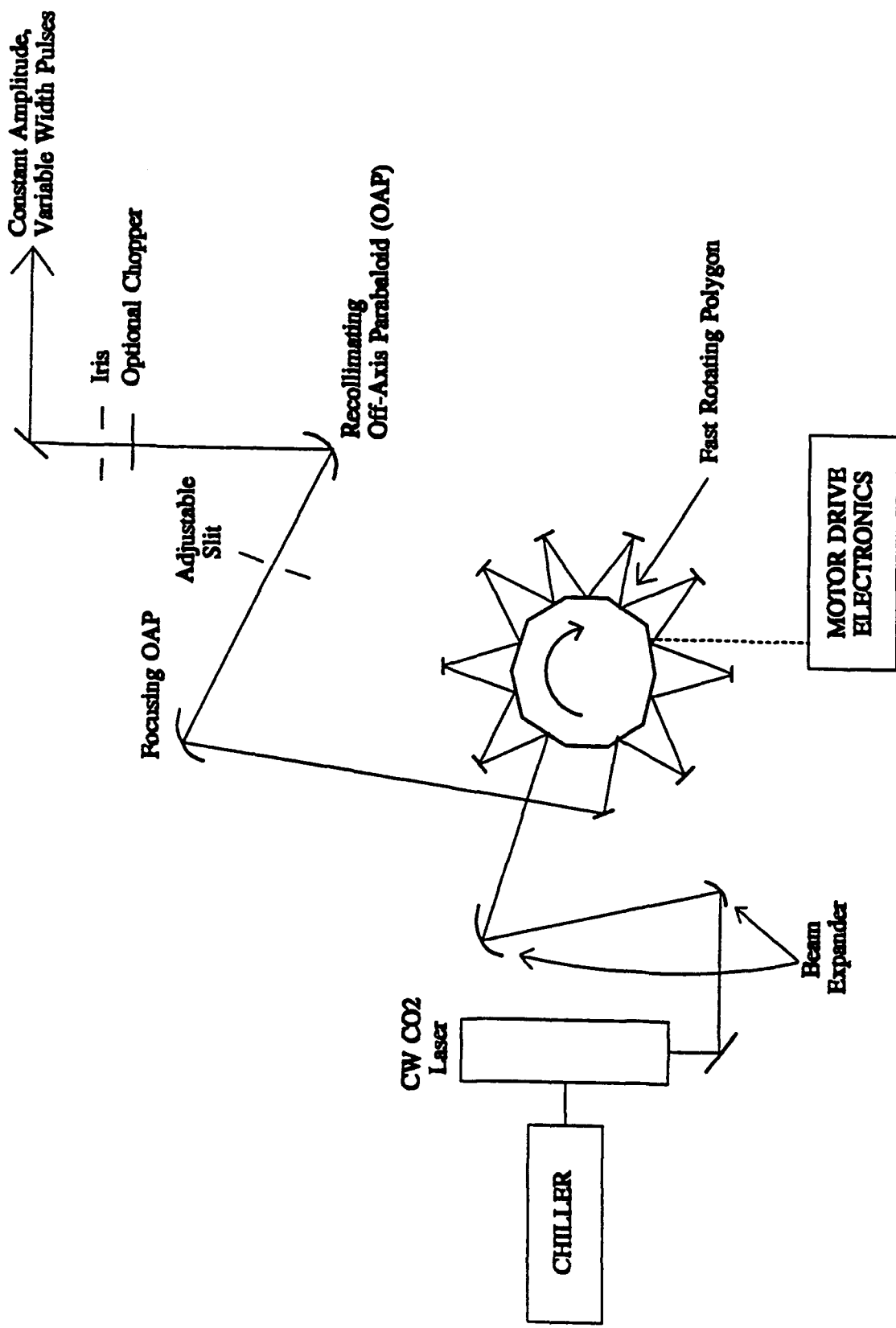


FIGURE 2-2. Polygon Scanner Layout

with a 0.25 mm MCT-pv detector with a 100 MHz amplifier.

A 4-step process was used to characterize each amplifier's rms noise. First, the amplifier noise was measured with a detector simulator circuit. This circuit had the correct resistance and capacitance to mimic the detector's electronic effect on the amplifier. Its schematic is shown in the appendix. Second, rms noise measurements were made with the detector connected to the amplifier's input. Third, these measurements were repeated with a single pole RC filter added to ensure that the circuit's bandwidth was the desired value. Finally, noise frequency spectra were taken using a spectrum analyzer at RL.

All three amplifier designs utilized a DC coupled preamplifier. Therefore, the DC current from the detector's response to background could be measured at the preamp's output. The noise contribution from the DC current is expected to be the generation-recombination (G-R) noise discussed in the literature⁽³⁾. A DC current of 1.2 microamps was detected in good agreement with the estimate of background flux in a room temperature laboratory.

2.5 Measurement Results

2.5.1 Pulse Attenuation Measurements

The polygon scanner-created pulses were characterized with the NERC detector with a 100 MHz preamplifier. Table 2-3 summarizes the pulsedwidths created with the device. Using nine mirror bounces, the pulsedwidth could be varied between 65 ns and 0.24 microseconds. To create a 1.0 microsecond pulse required using only one mirror bounce from the polygon. However, even with only a single bounce from the polygon, pulses approaching 10 microseconds could not be created. We recommend building a special single or two hole chopper blade which should be effective in creating the longer pulses. Measurement results for the short pulse experiments are summarized in Table 2-4. Absolute response, relative response (relative to chopped signal), and measured pulsedwidth are all reported. One microsecond pulse response measurements are shown in Table 2-5.

2.5.2 Noise Measurements

RMS noise measurements made for the various amplifier and detector combinations are shown in Table 2-6. Descriptions of the results are given in the text below.

3.5 MHz Noise Results

The wide band amplifier's noise is predicted to be dominated by the amplifier's voltage noise coupled through the detector's capacitance. Background noise is not expected to be a significant noise factor for this amplifier. Noise measurements confirmed that the noise level didn't vary as the background scene changed from hot (1000°C) to cold (<0°C). Adding an RC filter to the amplifier's final stage significantly reduced its noise, indicating some degree of excess bandwidth in the amplifier design.

TABLE 2-3. Measured Pulsewidths for Polygon Scanner

	Configuration 1			Configuration 2
Polygon Motor Drive Speed	50 Hz	120 Hz	320 Hz	105 Hz
100 MHz Module Pulsewidth (microseconds +/- 5%)	0.24	0.135	0.065	1.0

TABLE 2-4. Short Pulse Measurement Results

		Source Pulsewidth (Microseconds)			
Bandwidth	Quantity	286 (Chopped)	0.24	0.13	0.065
3.5 MHz	Response (Volts)	0.161	0.110	0.080	0.050
	Relative Response	1.0	0.68	0.50	0.31
	Measured Pulsewidth (Microseconds)	0.29	0.28	0.20	0.20
350 kHz	Response (Volts)	*	*	420	234
	Relative Response	*	*	*	*
	Measured Pulsewidth (Microseconds)	*	*	2.7	2.6
35 kHz	Response (Volts)	5.96	0.29	0.050	0.031
	Relative Response	1.0	.049	8.4×10^{-3}	5.2×10^{-3}
	Measured Pulsewidth (Microseconds)	286	10	9.3	6.5

* Data unreliable due to laser instability.

TABLE 2-5. One Microsecond Pulse Measurement Results

Bandwidth	Measured Response (+/- 5%)	Gain Corrected Relative Response	Pulsewidth
3.5 MHz	13 mV	1.0	1.0 μ s
350 kHz	160 mV	157 mV	2.8 μ s
35 kHz	36 mV		9 μ s

TABLE 2-6. Measured RMS Noise Currents

Amplifier	Configuration	RMS Noise Current	Comments
3.5 MHz	Simulator	31.2 nA	--
3.5 MHz	Simulator with RC filter with -3 DB at 2.7 MHz	16.6 nA	About twice the noise current expected
3.5 MHz	0.25 mm MCT-PV detector	29.6 nA	--
3.5 MHz	0.25 mm MCT-PV detector w/RC filter (2.7 MHz)	18.2 nA	Similar behavior to detector simulator
350 kHz	Detector simulator	4552 pA	--
350 kHz	Detector simulator with RC filter w/-3 DB at 265 kHz	415 pA	Nearly the same noise with and without RC filter
350 kHz	0.25 mm MCT-PV detector	7.5 nA	Roughly 15 times larger than expected increase in noise going to detector
350 kHz	0.25 mm MCT-PV detector w/RC filter (265 kHz)	6.5 nA	--
350 kHz	0.5 mm MCT-PV detector	16 nA	Noise strongly affected by larger area detector
350 kHz	0.5 mm MCT-PV detector w/RC filter (265 kHz)	15 nA	--
35 kHz	Detector simulator (preamplifier gain = 10^7 ohms)	13.2 pA	
35 kHz	Detector simulator with RC filter w/-3 DB at 21.8 kHz (preamplifier gain = 10^7 ohms)	12.0 pA	
35 kHz	0.25 mm detector (preamplifier = 10^7 ohms)	--	Preamp saturated with detector DC current
35 kHz	Detector simulator (preamplifier gain = 10^6 ohms)	65 pA	Reduction in feedback resistor raises Johnson noise
35 kHz	0.25 mm detector (preamplifier gain = 10^6 ohms)	5 nA	Roughly 15 times larger than expected increase in noise going to detector
35 kHz	0.5 mm detector (preamplifier gain = 10^6 ohms)	--	Preamp saturated with DC current

Figure 2-3 shows the noise spectrum of the 3.5 MHz amplifier which reveals an unusual feature at 400 kHz with a large decrease in noise between 400 kHz and 2 MHz. The lower bandwidth limit for the amplifier was several hundred Hertz, so a structured noise spectrum, such as this, was not anticipated. The noise spectrum was the same with the detector simulator.

350 kHz Noise Results

The 350 kHz detector/preamp combination exhibited significantly more noise than predicted. The rms noise associated with the detector's 1.2 microamp DC background current is 370 pA, which should be a noticeable contribution to the total noise. However, when hooked to a detector, the total rms noise increased to 7.5 nA which is over an order of magnitude higher than the expected total noise. Adding an RC filter to the system decreased the noise only slightly indicating that the problem was not excess bandwidth. A frequency spectrum of the system's noise, shown in Figure 2-4, reveals a large feature at 460 kHz. The additional features present at higher frequencies are simply harmonics of the 460 kHz peak. The noise spectrum with the detector simulator attached is much more benign, as shown in Figure 2-5. There seems to be a slight peaking near 250 kHz, but the noise magnitude is much lower and there is no dominant noise feature.

To test if the amplifier's frequency response was the problem, the amplifier was attached to a sine wave generator to measure amplitude as a function of frequency. Table 2-7 presents the results of the test which indicate that the amplifier is behaving properly. No unusual signal gain is seen at 460 kHz. This observation suggests that the problem relates to the detector's influence on the circuit which is, apparently, more complicated than the detector simulator circuit built to mimic its electrical characteristics.

35 kHz Noise Results

Initially, measurements were made with the 35 kHz preamp connected to the detector simulator. Predictions of the nominal noise level were 9.6 pA rms which compared favorably to the 13.2 pA measured with the amplifier. Predictions more accurate than this are not practical without characterizing all of the stray capacitance sources such as wires and connections between the amplifier and detector. A slight noise reduction was observed when a 31.8 kHz RC filter was added to the system. Since the detector's DC background current was over a microamp, the high gain preamp was driven to saturation when hooked to the detector. Therefore, the 10⁷ ohm feedback resistor was reduced to 10⁶ ohms to avoid saturating the preamp. The rms noise voltage with the modified preamp attached to the detector simulator was lower due to the feedback resistance reduction, even though the actual noise current value was higher. Lowering the feedback resistor increases this component's Johnson noise.

As with the 350 kHz amplifier, the rms noise voltage was dramatically higher than predicted with the detector attached. Specifically, we anticipated a noise increase to 7.4 mv rms due to the DC current shot noise. However, we measured an increase to 70-100 mv noise rms with the detector attached. The frequency spectra for the detector simulator and actual detector are shown in Figures 2-6 and 2-7, respectively.

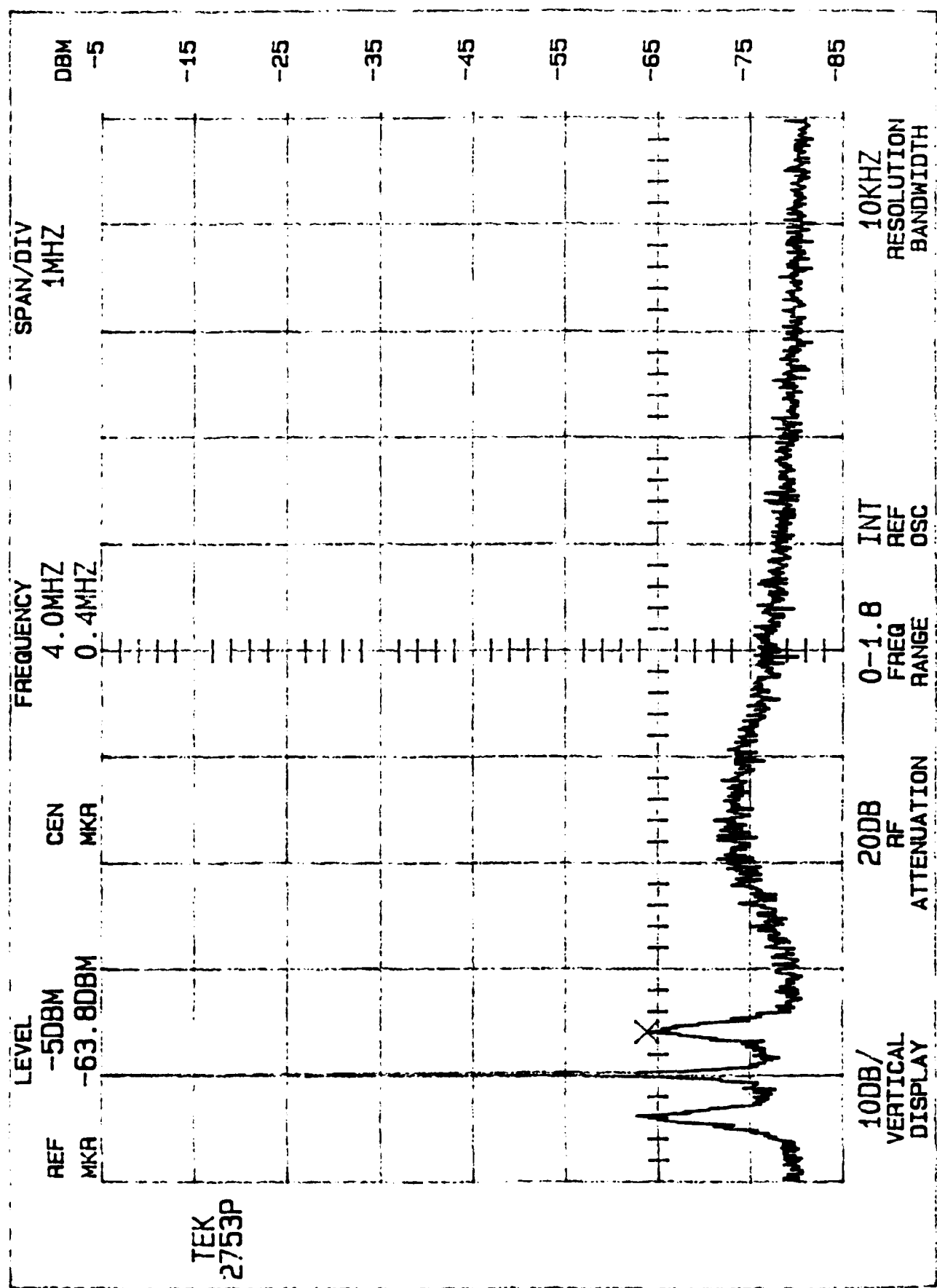


FIGURE 2-3. Noise Spectrum of 3.5 MHz Amplifier and 0.25 mm Detector

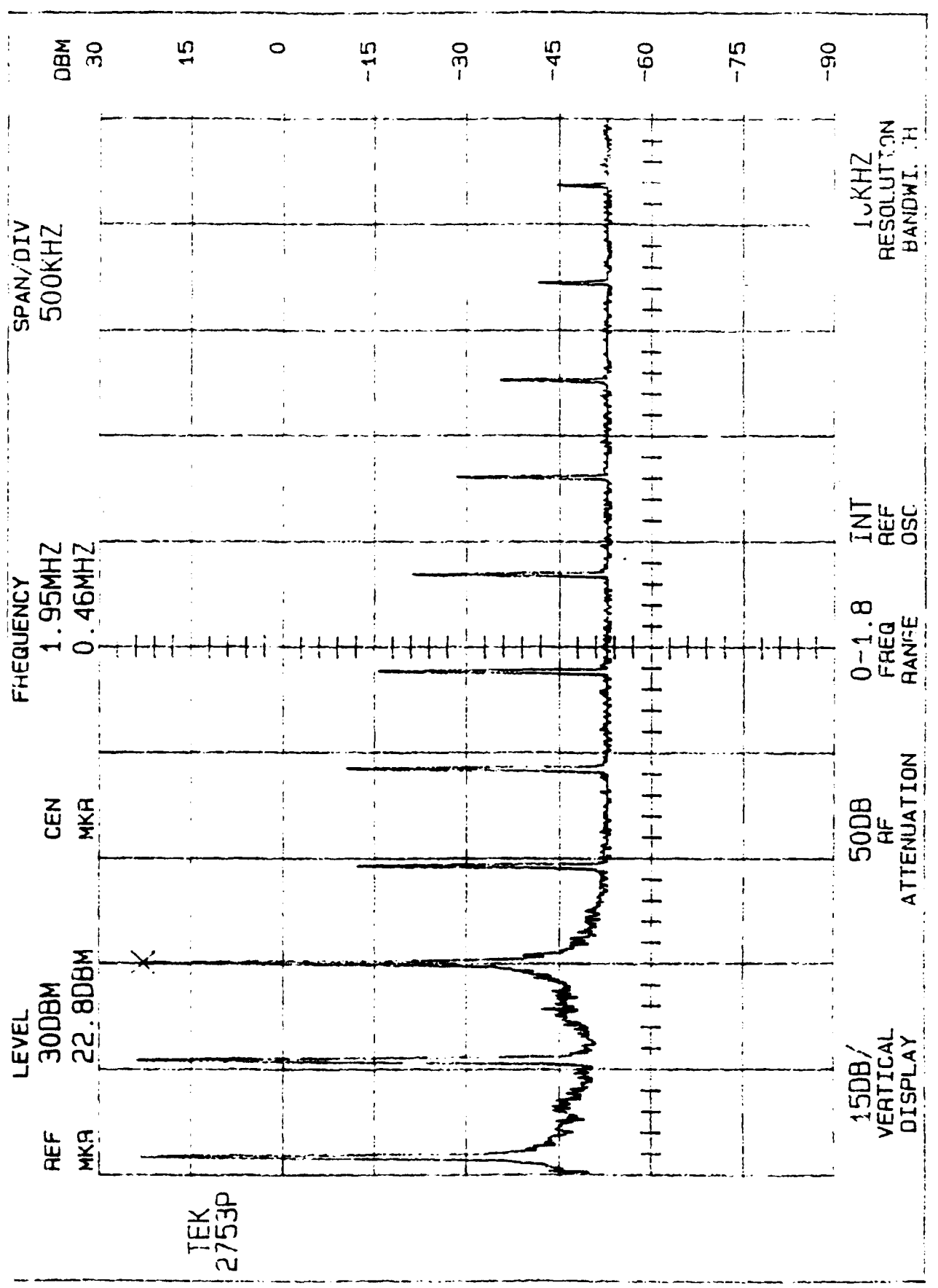


FIGURE 2-4. Noise Spectrum of 350 kHz Amplifier and 0.25 mm Detector

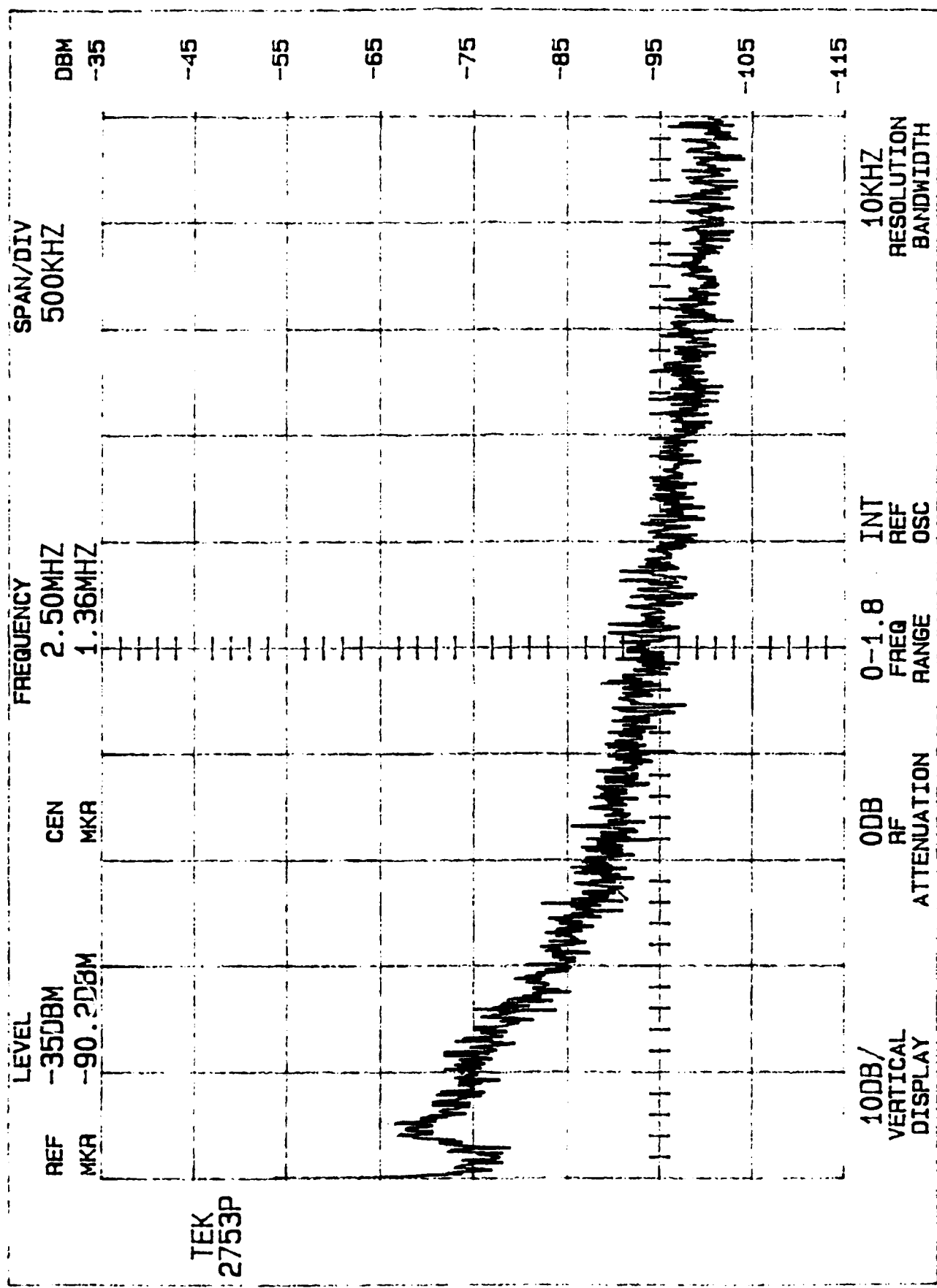


FIGURE 2-5. Frequency Spectra of 350 kHz Amplifier and Detector Simulator

TABLE 2-7. Sine Wave Response of 350 kHz Amplifier

Frequency (kHz)	Amplitude (mv)
0.5	15
1.0	28
2.0	52
10	135
30	158
48	155
63	160
93	163
97	159
155	170
200	182
300	170
350	129
275	108
405	91
425	74
450	63
500	52
600	28

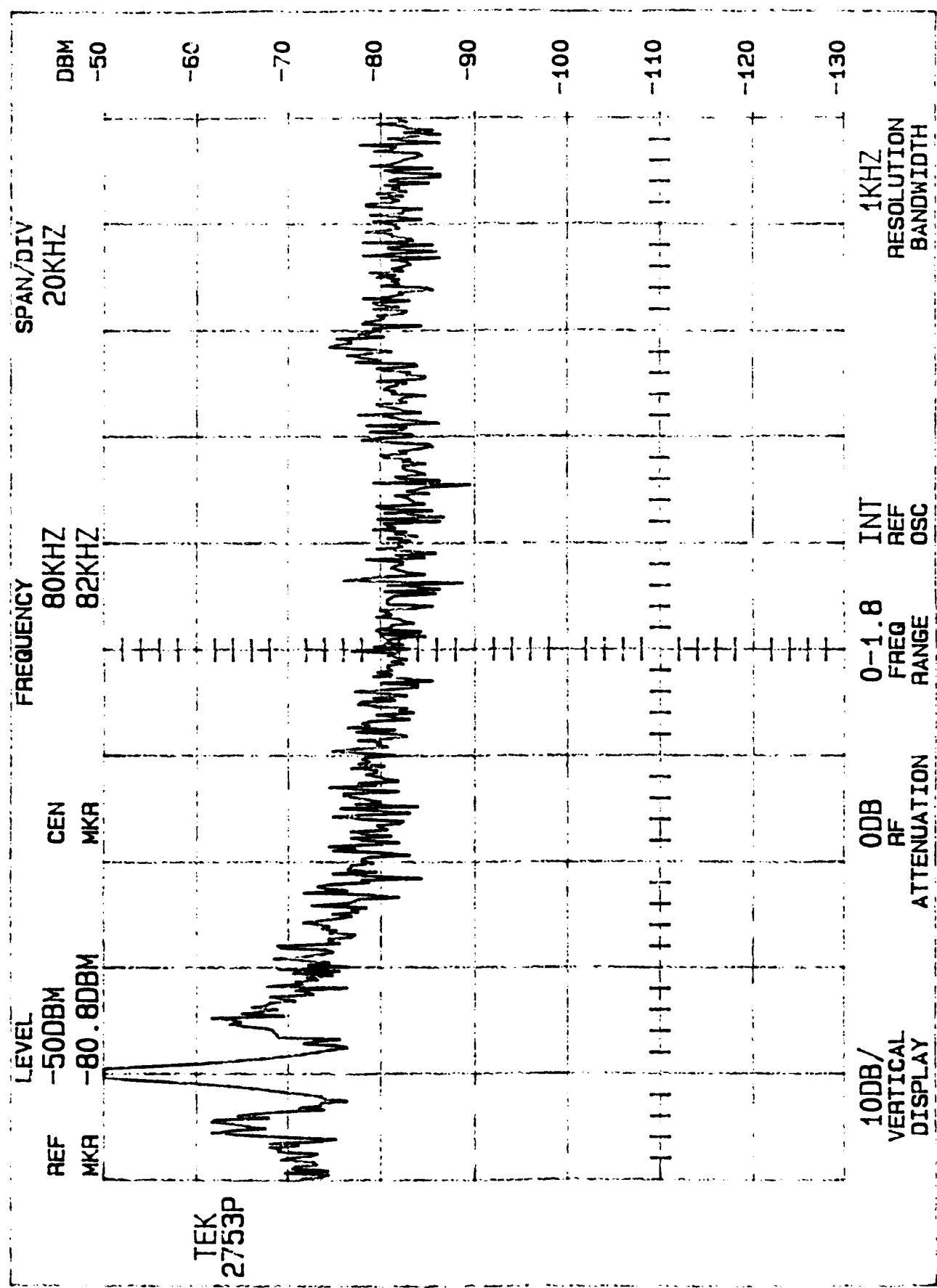


FIGURE 2-6. Noise Spectrum for 35 kHz Amplifier and Detector Simulator

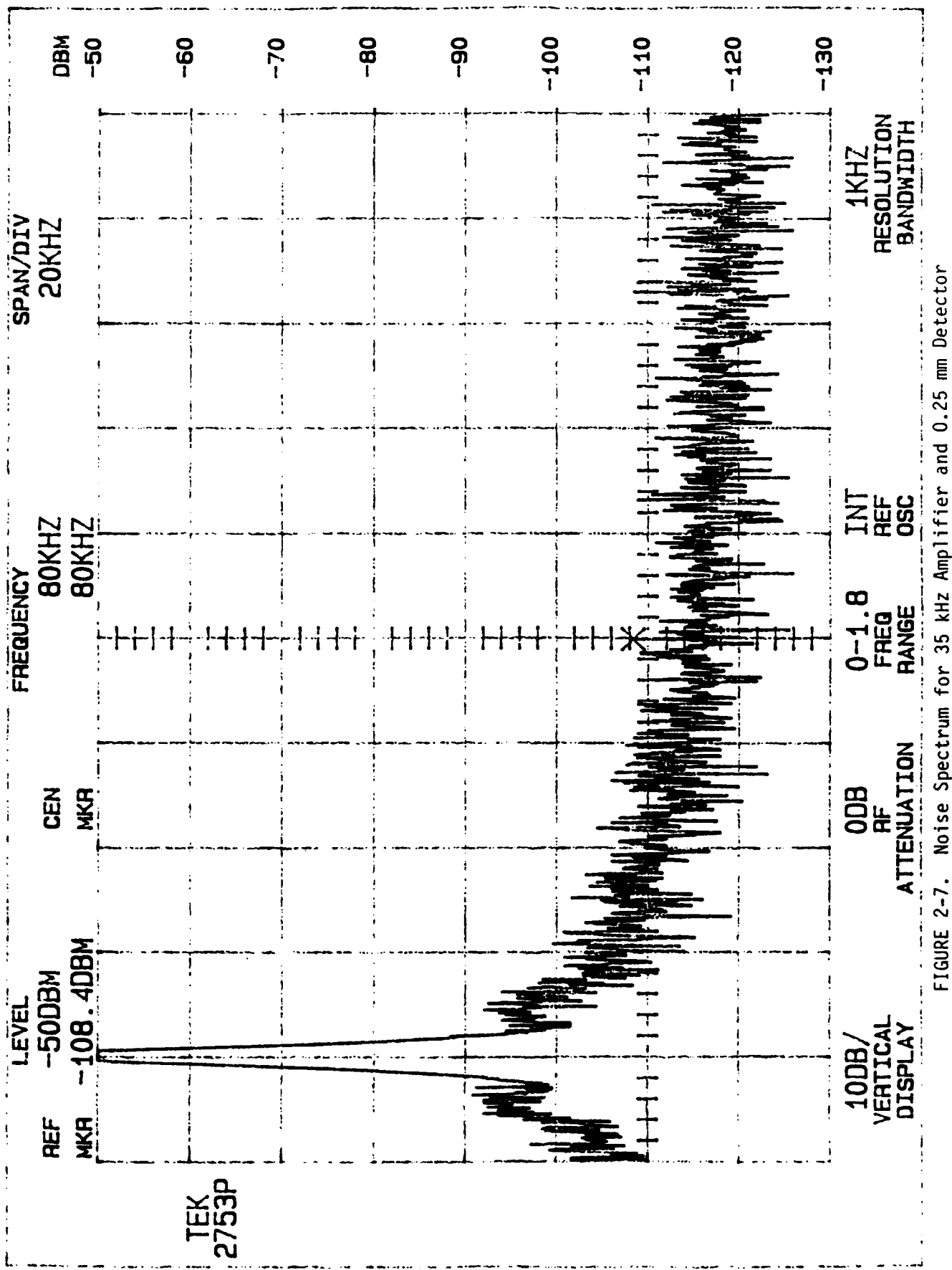


FIGURE 2-7. Noise Spectrum for 35 kHz Amplifier and 0.25 mm Detector

2.5.3 CNVEO System Sensitivity

The CNVEO system threshold was determined using the polygon scanner to create short pulses of radiation. The DIA AOTF radiometer was used to measure the flux from a sandpaper target. Initially, the CNVEO system was placed approximately 30 feet from the sandpaper and pointed to the target. Next, the intensity of the pulses was decreased by reducing the slit width on the polygon scanner. This procedure is effective once the slit width is smaller than the laser spot. The intensity was reduced until the system's indicator light was flashing only sporadically. Then the AOTF radiometer was put in the same position as the CNVEO system to measure the flux. Since the AOTF radiometer has a bandwidth of only 80 kHz, the polygon needed to be stopped and positioned in the CW mode. The chopped signal was measured to quantify the W/cm^2 incident at the aperture. The system's threshold was measured to be $5 \times 10^{-10} \text{ W/cm}^2$. The system's threshold was not strongly affected by changes in the source pulselwidth from 65 ns-240 ns. It did not detect the chopped signal at ~1 kHz.

2.6 Conclusions

While the pulse attenuation data validated the model predictions, the measured noise values were significantly higher than predicted. The noise discrepancy is particularly significant since the RL measurement scenario requires a high sensitivity receiver. Losing an order of magnitude of sensitivity due to unexpected noise sources will reduce the effective range of the scenario. However, the strong spectral structure of the noise may indicate that the problem is readily solvable. The problem is likely attributable to an electrical instability induced by the actual detector characteristics which are only approximated by the detector simulator. Electronic instabilities of this type are usually corrected by adding select components to dissipate the unstable frequency. Given the importance of the receiver's sensitivity to the RL mission, correcting this problem should be a high priority in a future effort.

3. COSMIC RAY DETECTION EXPERIMENT

3.1 Objectives and Approach

The cosmic ray detection measurements were made to estimate rates and magnitudes of cosmic ray events from MCT detectors. Cosmic rays are important false alarm sources which must be distinguished from lasers by laser detection sensors. The two most common ways to reject cosmic ray false alarms are coincidence detection and pulselength discrimination. Coincidence detection uses two detectors which must record signals simultaneously. If only one sensor records an event, it is assumed to be a cosmic ray or a spurious noise source. The two sensors must be separated on the order of an inch or more since cosmic rays reaching the earth's surface typically consist of high energy electron showers which can affect neighboring detectors in an array.

The experimental approach taken to characterize the MCT cosmic rays was to use a high speed digital oscilloscope (Phillips 3323) to capture threshold crossing events. A threshold level of 8-10 times the NEI noise level was used to avoid spurious noise pulses. Measured traces were downloaded to a PC-compatible computer via an RS-232 link using a program written under this effort. The digitized traces were later plotted and analyzed. Experiments typically were run for several hours at a time with the equipment unattended on a lab bench. A cover was placed over the optics to avoid stray pulses from optical sources.

3.2 Experimental Results

Table 3-1 summarizes the detectors used for the cosmic ray experiment. Silicon, photovoltaic MCT, and photoconductive MCT were all tested. Table 3-2 presents an overview of the experiments carried out at SciTec. Threshold crossings consisted of cosmic ray events, power line glitches, and spurious electronic noise sources.

Figures 3-1 and 3-2 show the MCT-PV response to typical cosmic rays and noise glitches. The cosmic ray produces a characteristic impulse response which could easily be confused with radiation sources. The noise glitch can be rejected based on the pulse shape and symmetry of the curve around the zero line. Typical amplifier noise response measurements without the detector attached are shown in Figures 3-3a and b. Figures 3-4 a through c present a number of noise glitch events and two cosmic rays with the MCT detector and a 100 MHz amplifier.

The noise glitches show how important it is to characterize the environment in which the sensor will operate. Noise rejection schemes using the symmetry or frequency content of the events could be used to reject them. However, solving laboratory noise problems for an airborne system may not address the problems found in the actual environment. At RL, new noise pulses were seen, possibly associated with RF devices in the vicinity. Sufficient time was not available to systematically characterize the noise pulses at RL. Future efforts should measure the noise environment, particularly in the field and in the air, in the vicinity of RL.

TABLE 3-1. Detector Characteristics

Detector	Material	Bandwidth (MHz)	Area (cm ²)	Active Area Shape
SNL-APD 8616-PC 8616-PC	Si	20/0.5	0.071	3 mm round
	Si	10	0.887	1.06 cm round
	Si	0.01	0.887	1.06 cm round
NERC-MCT AOTF-MCT MCT-RFB	HgCdTe	100	6.25E-4	0.25 mm square
	HgCdTe	0.08	0.0314	2 mm round
	HgCdTe	10/0.5	0.0314	2 mm round

TABLE 3-2. Summary of Cosmic Ray Runs

Date, Run	Radiometer	Bandwidth (MHz)	# of Event	Time (Hrs)
05/15 A	NERC-MCT	100	4	1.212
05/15 B	NERC-MCT	100	8	4.429
05/16	NERC-MCT	100	18	5.876
05/17 A	NERC-MCT	100	9	6.057
05/17 B	DIA-APD	20	12	0.515
05/17 C	DIA-APD	20	15	0.376
05/20 A	DIA-APD	20	35	1.292
05/20 B	DIA-APD	20	38	1.037
05/20 C	8616-PC	0.01	43	0.848
05/20 D	8616-PC	0.01	23	1.898
05/20 E	8616-PC	0.01	29	1.956
05/20 F	8616-PC	10	40	0.533
05/21 A	8616-PC	10	22	1.542
05/21 B	8616-PC	10	39	3.329
05/21 C	DIA-APD	20	35	1.097
05/21 D	DIA-APD	20	2	0.724
05/21 E	DIA-APD	0.5	15	0.388
05/21 F	DIA-APD	0.5	17	0.414
05/22 A	DIA-APD	0.5	193	5.882
05/22 B	NERC AMP only	100	52	2.417
05/22 N	NERC AMP only	100	18	14.448
05/23 A	NERC-MCT	100	21	5.186
05/23 N	DIA-APD	0.5	7	16.470
05/24	DIA-APD	0.5	216	6.961
05/28 A	DIA-APD	0.5	12	0.313
05/28 B	DIA-APD	0.5	179	7.805
05/28 N	8616-PC x10	0.01	151	18.196
05/29 A	8616-PC x100	0.01	78	5.056
06/03 A	AOTF-MCT	0.08	0	1.327
06/03 B	AOTF-MCT	0.08	14	1.331
06/03 C	AOTF-MCT	0.08	22	4.049
06/05	AOTF-MCT	0.08	55	1.786
06/06 A	AOTF-MCT	0.08	70	3.277
06/06 B	AOTF-MCT	0.08	49	2.044
06/06 N	AOTF-MCT	0.08	133	11.760
06/13 A	AOTF-MCT	0.08	56	3.435
06/13 B	AOTF-MCT	0.08	54	3.539
06/17	AOTF-MCT	0.08	31	2.425
06/18	AOTF-MCT	0.08	23	1.714

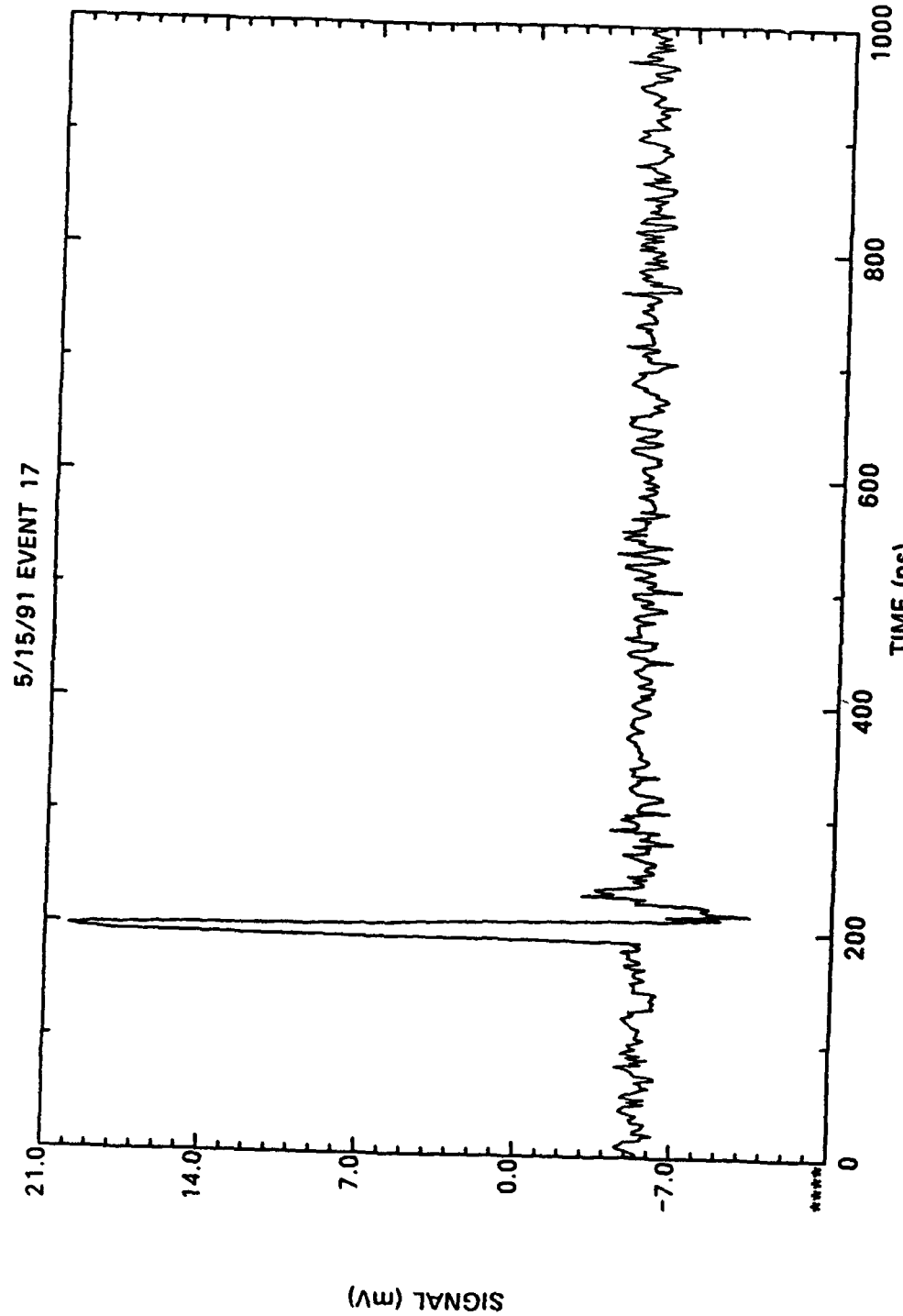


FIGURE 3-1. COSMIC RAY RESPONSE OF NERC MCT-PV SECTOR

PDM_POST
16-MAY-91 12:46:05

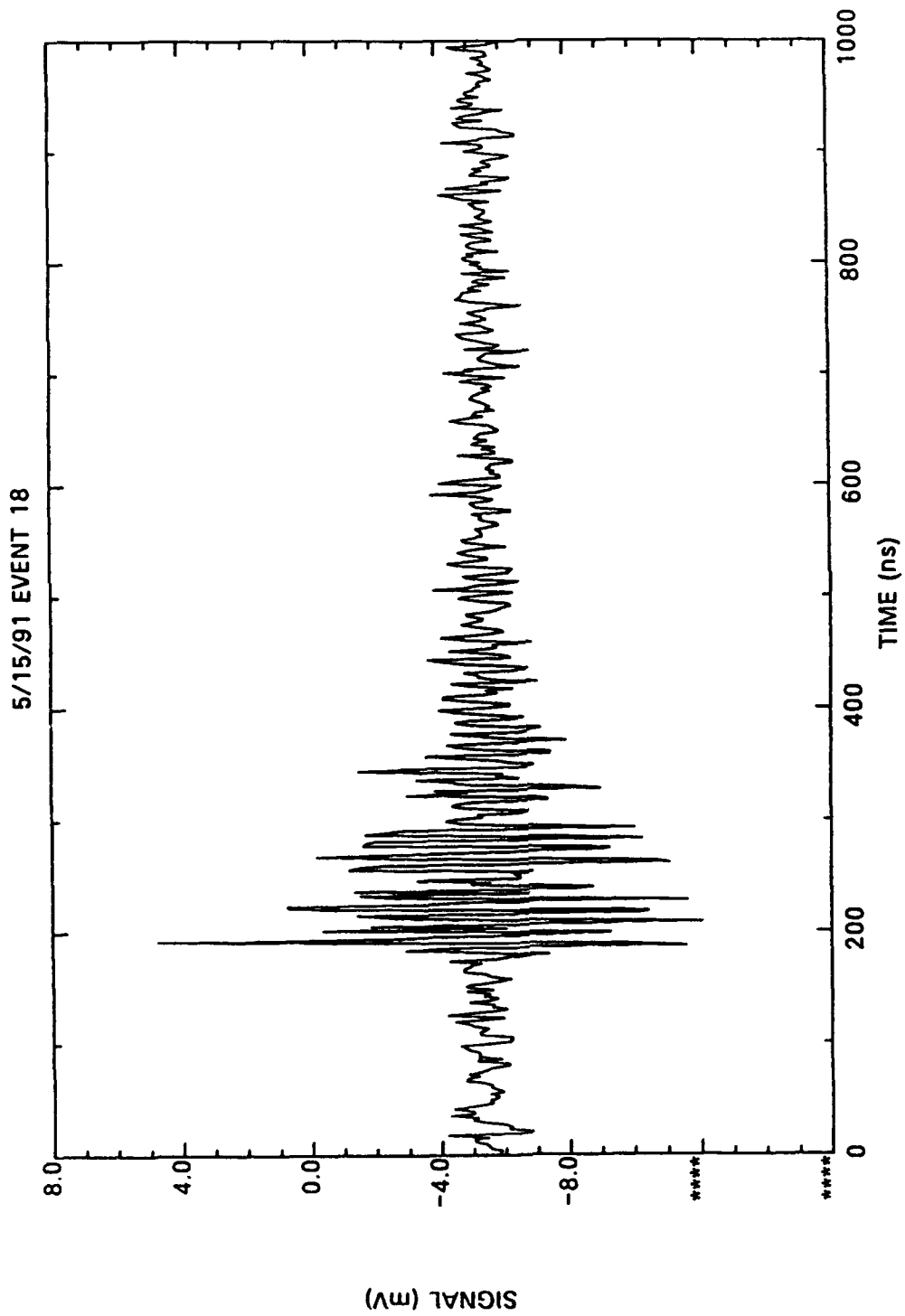


FIGURE 3-2. NOISE GLITCH ON NERC MCT-PV

PDH_ROST
16-MAY-91 12:46:28

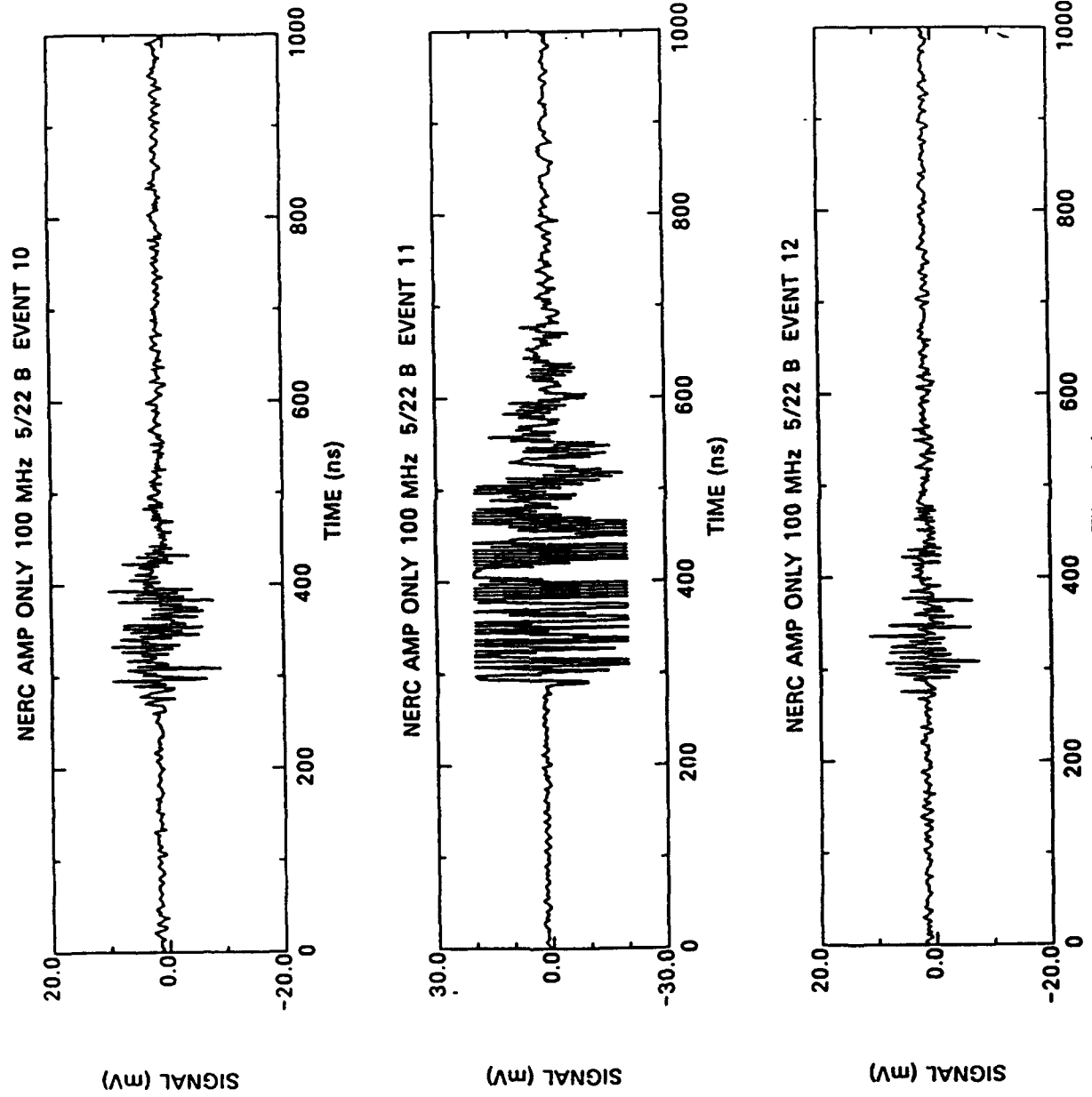


FIGURE 3-3a. NERC AMPLIFIER RESPONSE TO NOISE GLITCHES
23-MAY-91 09:48:29
PDH ROST

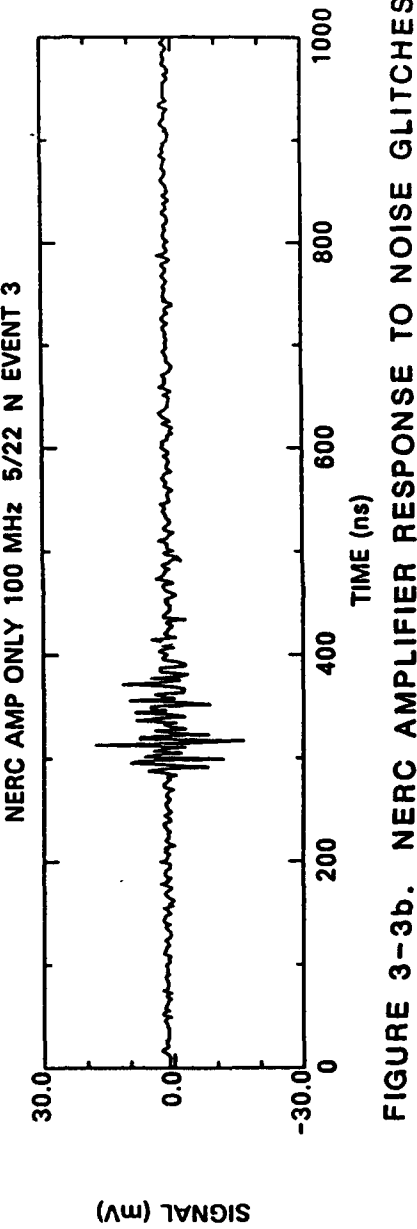
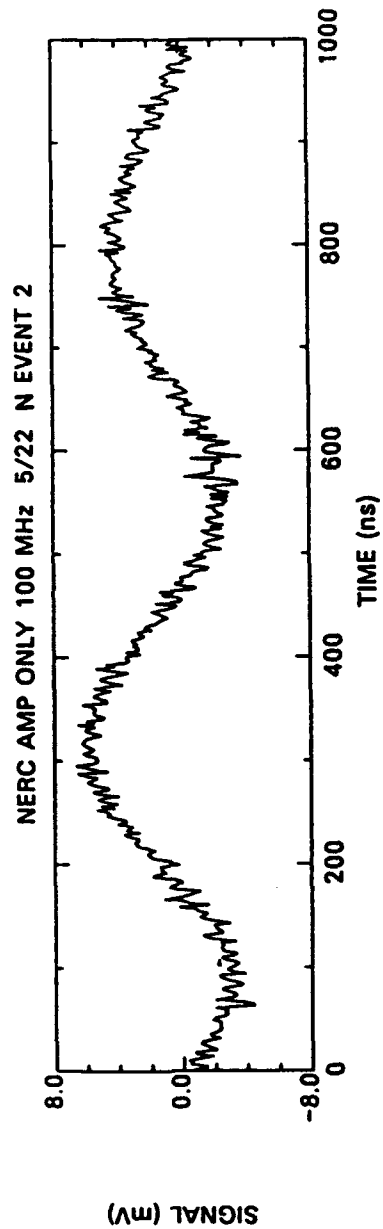
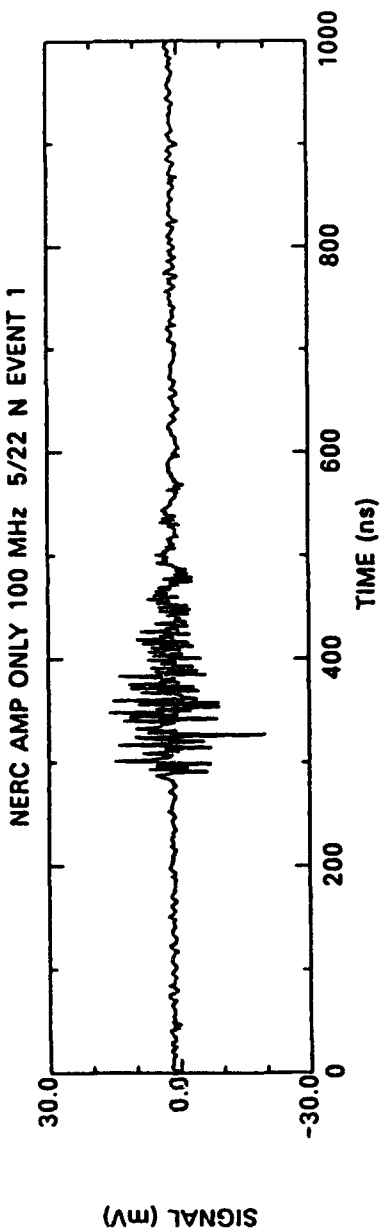


FIGURE 3-3b. NERC AMPLIFIER RESPONSE TO NOISE GLITCHES

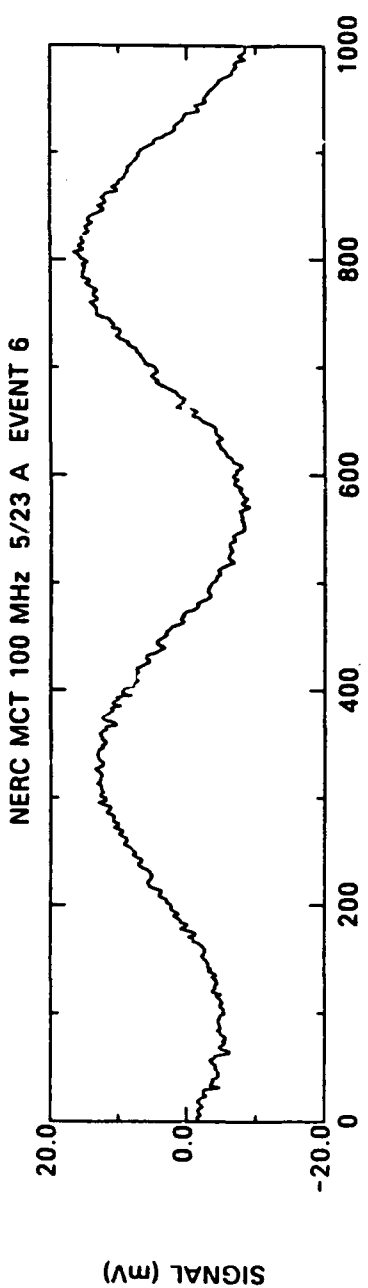
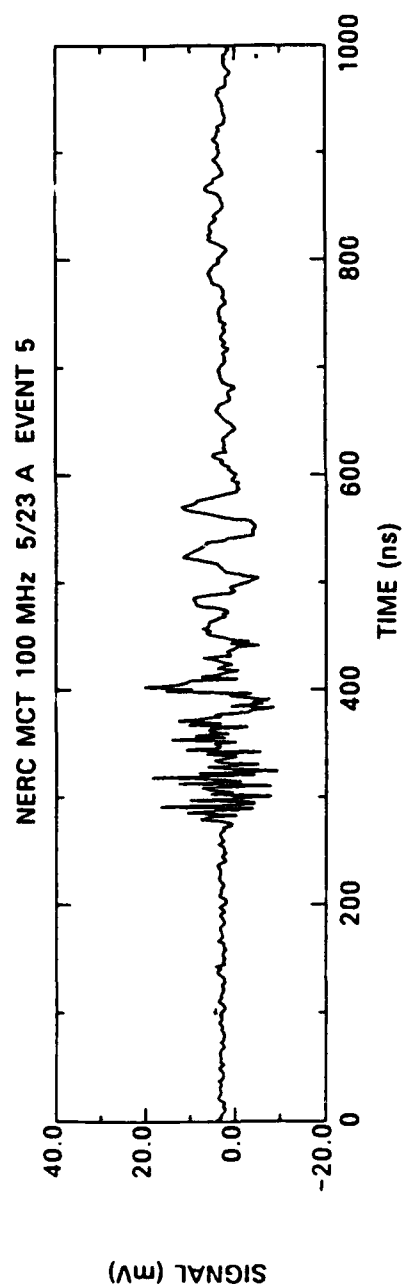
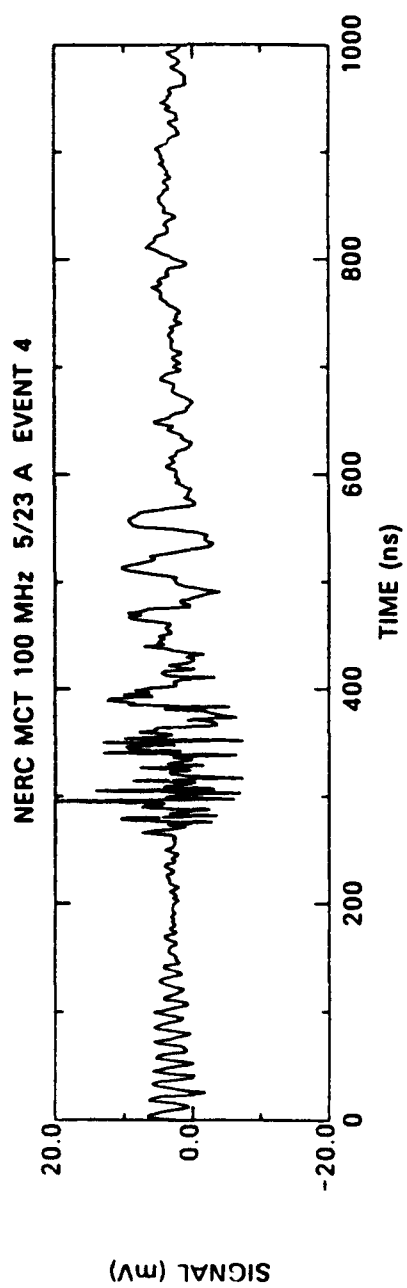
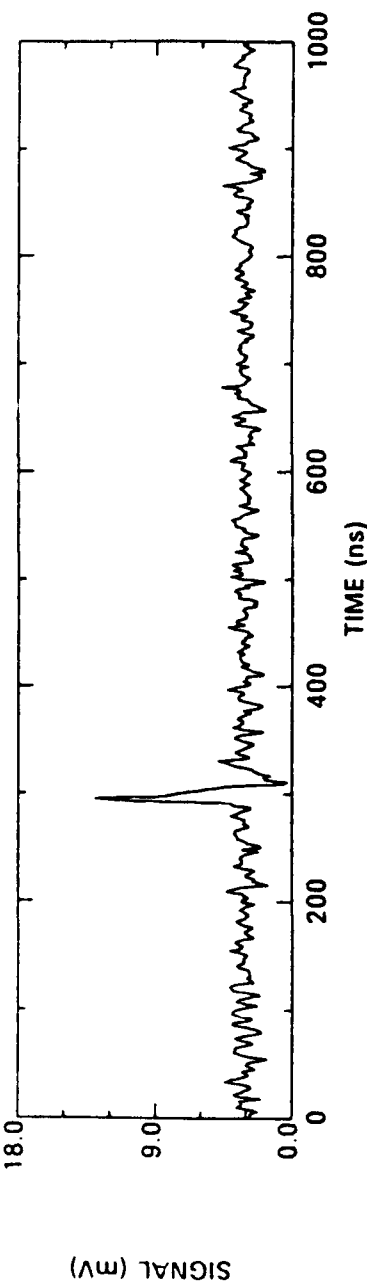


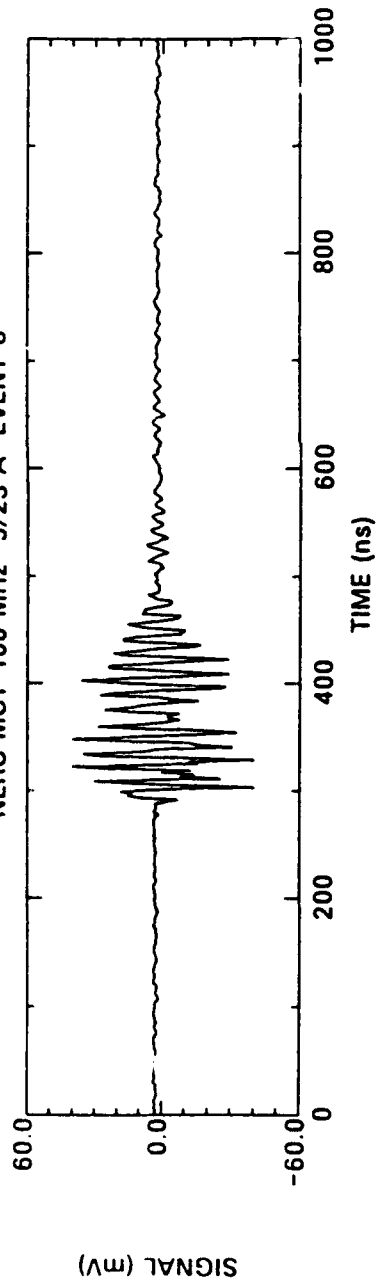
FIGURE 3-4a. NOISE PULSE MEASUREMENTS WITH
NERC DETECTOR AND 10J MHz AMPLIFIER

PDH_ROST
24-MAY-91 10:54:27

NERC MCT 100 MHz 5/23 A EVENT 7



NERC MCT 100 MHz 5/23 A EVENT 8



NERC MCT 100 MHz 5/23 A EVENT 9

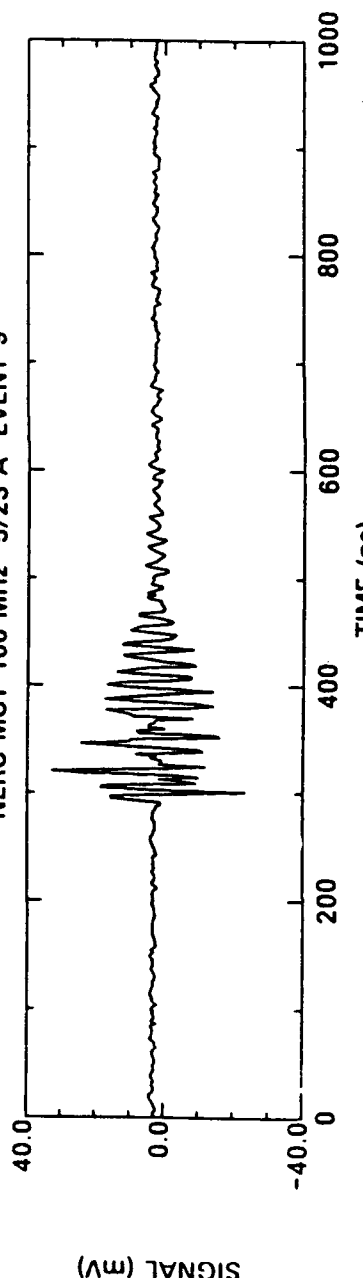


FIGURE 3-4b. NOISE PULSE MEASUREMENTS WITH
NERC DETECTOR AND 100 MHz AMPLIFIER
24-MAY-81 10:55:41
PDH_R0ST

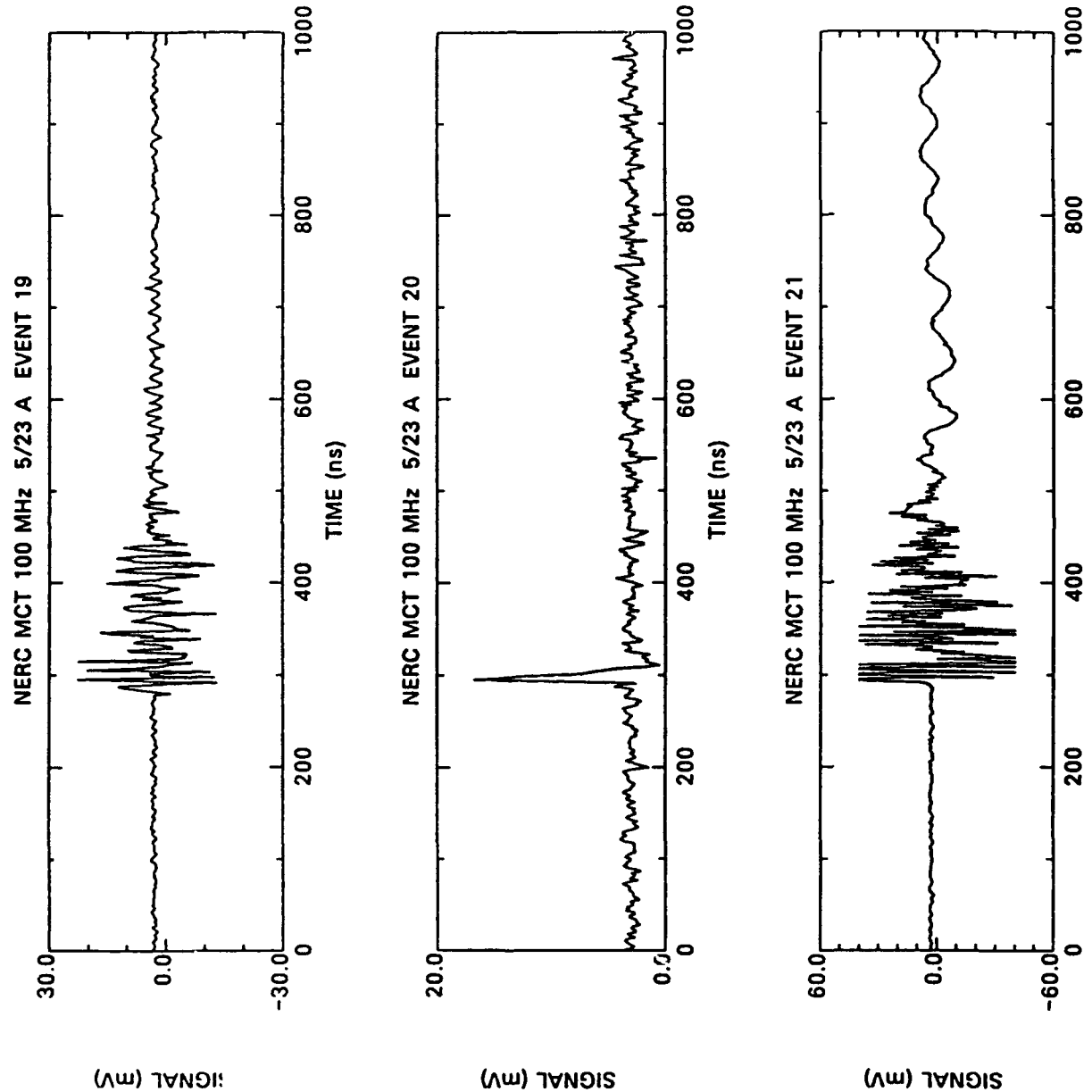


FIGURE 3-4c. NOISE PULSE MEASUREMENTS WITH
NERC DETECTOR AND 100 MHz AMPLIFIER

PDH_ROST
24-MAY-91 10:59:37

Figures 3-5a through 3-5c present a variety of noise pulses exhibited by a silicon APD detector with a 20 MHz bandwidth. This type of detector is suitable for measuring 20 ns laser pulses such as rangefinders and designators. A wide range of amplitudes were seen in the plots indicating that amplitude thresholding techniques alone would be ineffective in rejecting cosmic rays. All of the cosmic ray pulses were virtually identical in shape.

Figures 3-6a and 3-6b show results of the same APD detector at a bandwidth of 0.5 MHz. The receiver in this configuration has been used in the past to increase receiver sensitivity when atmospheric and geometric effects broadened a 20 ns laser pulse to hundreds of nanoseconds. Cosmic ray events were significantly broadened as expected. Interestingly, we observed a number of effectively shorter events due to spurious electrical noise signals. These threshold crossings fall well below the expected minimum received pulselength based on the receiver bandwidth and could, therefore, be rejected on pulselength grounds.

A 10 kHz silicon receiver, on Sandia tests, used to measure 0.5 msec pulses from B-36 was tested for its cosmic ray response. The measurements are presented in Figures 3.7a through 3.7d. Like the reduced bandwidth APD detector, broadened pulses are seen in response to cosmic rays. Also, a number of very short noise spikes are seen which could be rejected on pulselength grounds.

Figures 3.8a through 3.8f show threshold crossings for a MCT photoconductive detector with an 80 kHz amplifier. This detector showed somewhat less amplitude variation in its cosmic ray response than the previous detectors. However, it was the only one to exhibit pulselength variations.

Summary

Cosmic ray rates were estimated from the threshold crossings by discounting the events which were due to noise glitches, dividing by the sample interval, and normalizing by detector area. The rates for each detector are summarized in Table 3-3.

3.3 Conclusions

The deduced cosmic ray rates varied considerably depending on the detector material, the sensor bandwidth, and the sample interval. The most consistent measurements were with the DIA APD detector module. At 10 kHz, the 8616-PC module exhibited a significantly lower cosmic ray rate than the APD. This difference may be attributable to the 8616-PC's lower bandwidth which attenuates the impulse response cosmic rays severely. However, the photoconductive pin diode is significantly different in design than the APD and wider bandwidth pin diode measurements are warranted.

The NERC MCT-PV detector produced nearly an order of magnitude more cosmic rays per unit area of detector than the silicon APD. The reason for this discrepancy needs to be further

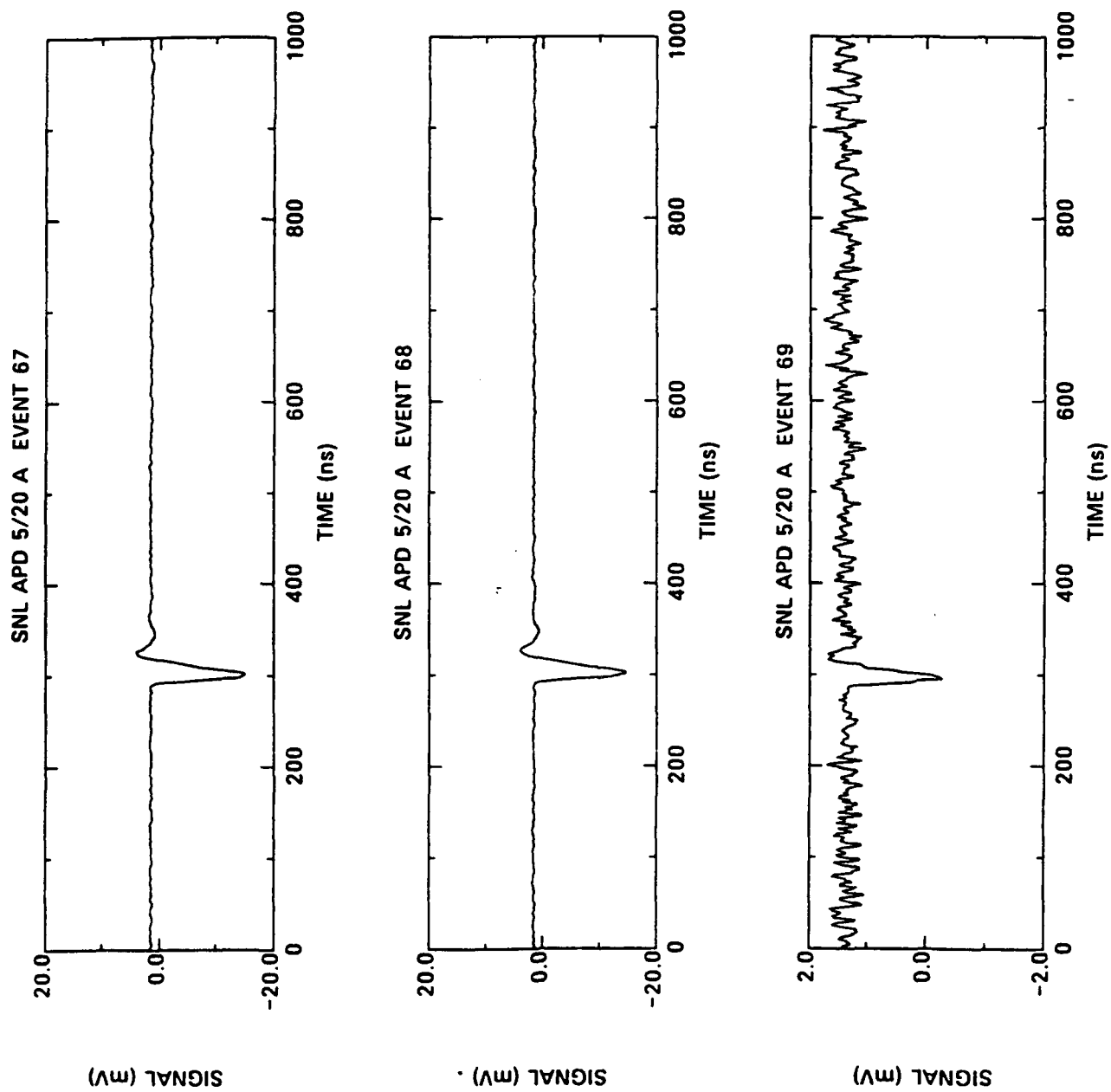


FIGURE 3-5a. 20 MHz SILICON APD NOISE RESULTS

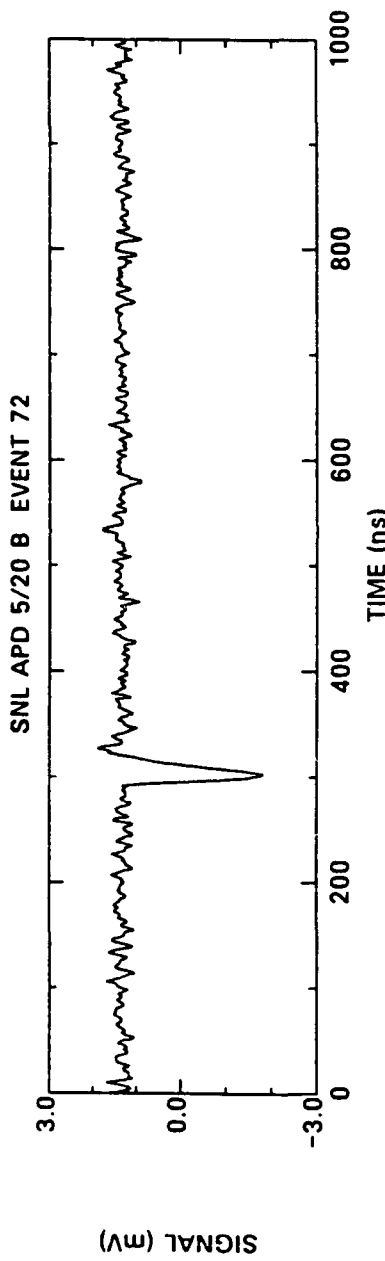
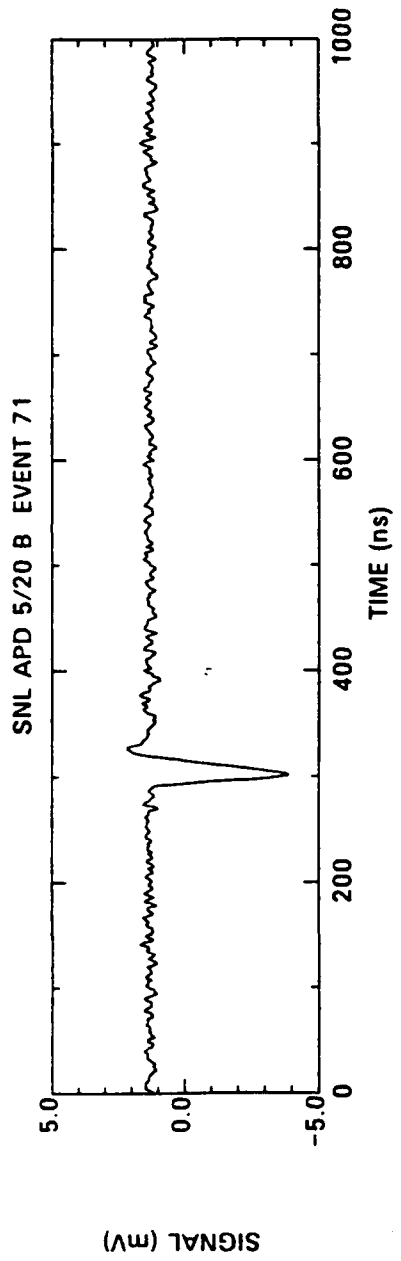
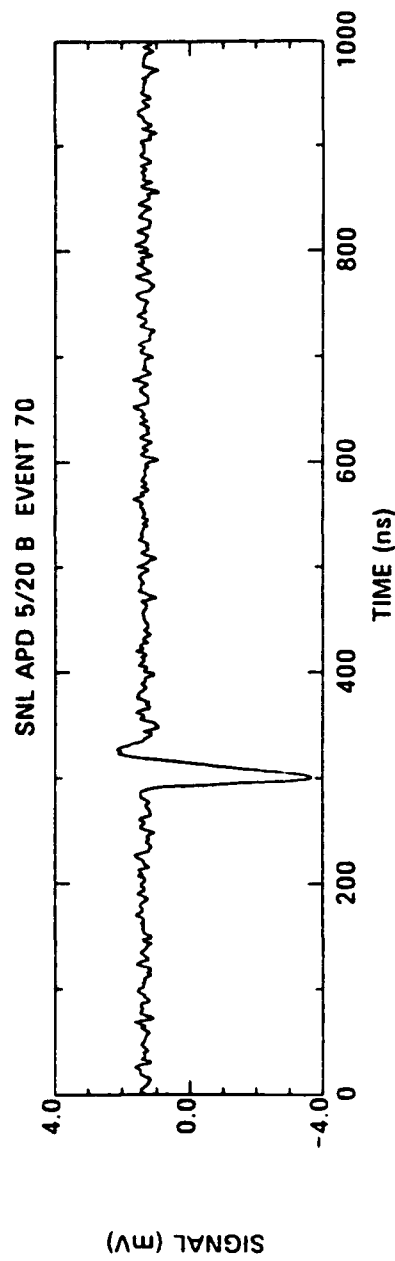
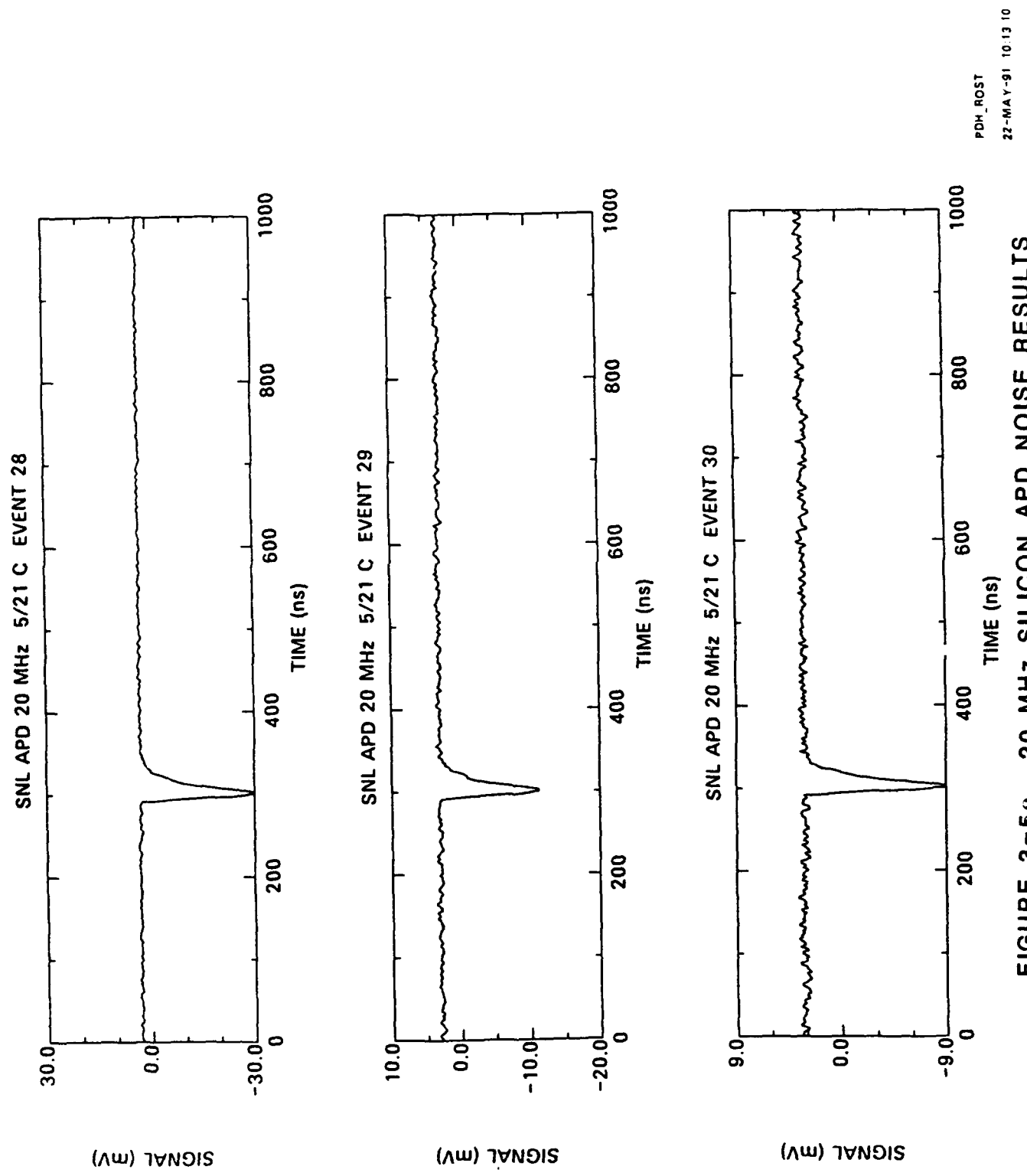


FIGURE 3-5b. 20 MHz SILICON APD NOISE RESULTS



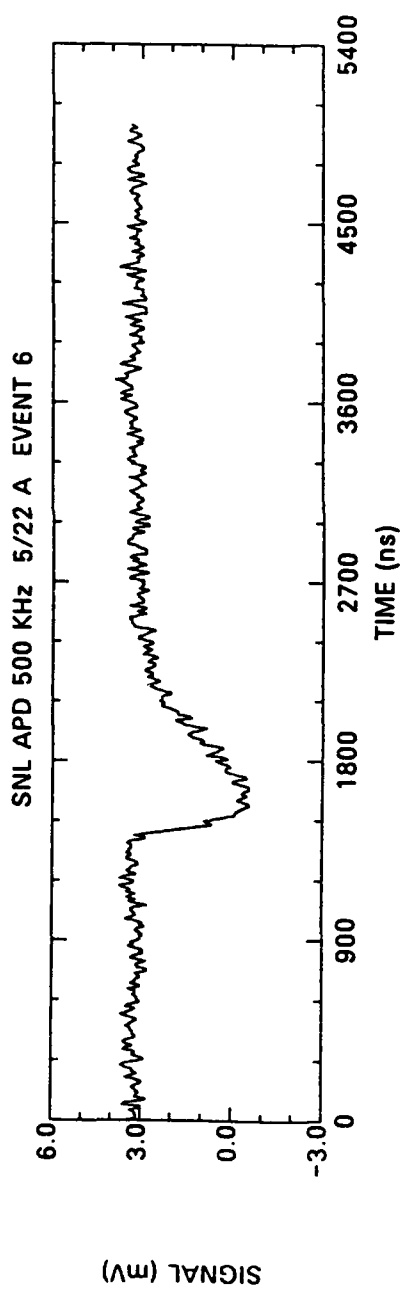
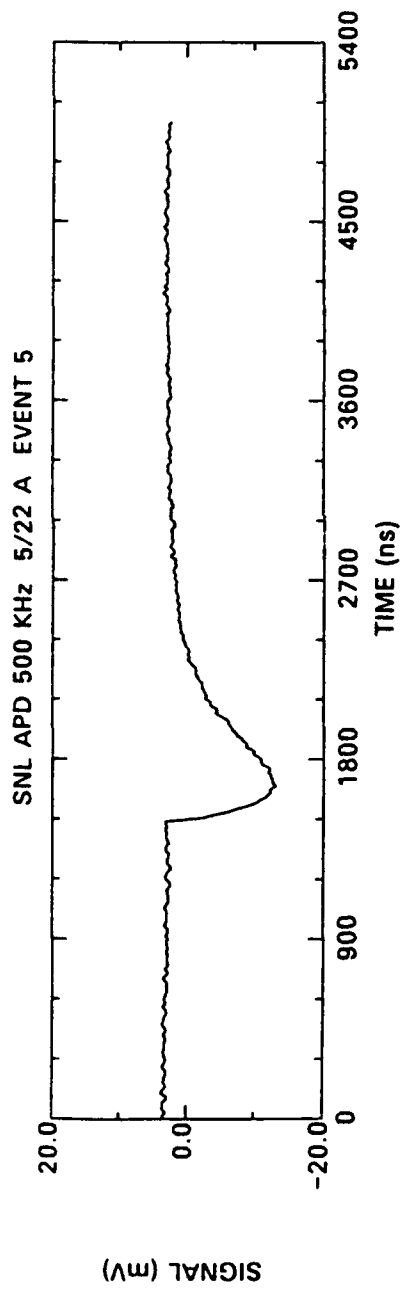
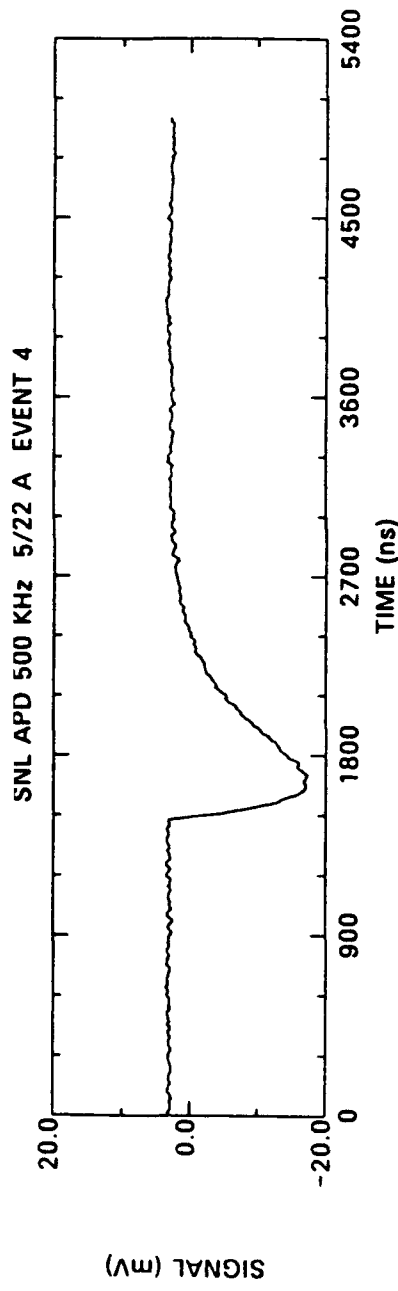


FIGURE 3 - 6a. 0.5 MHz SILICON APD NOISE RESULTS

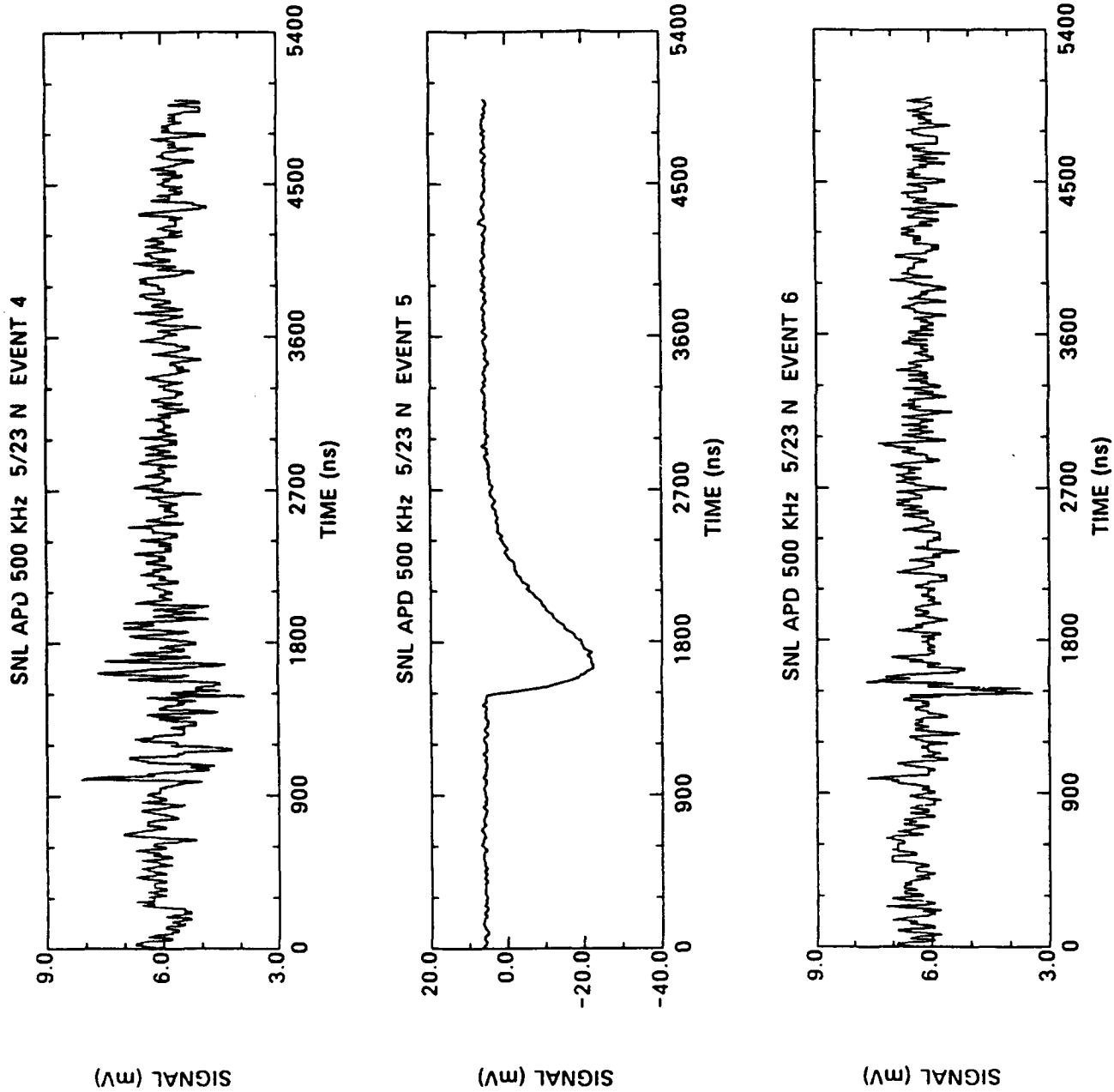
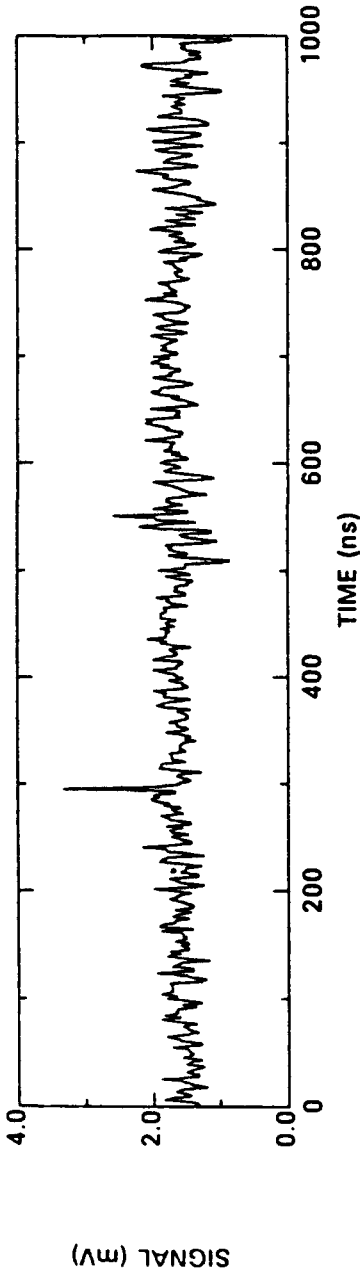


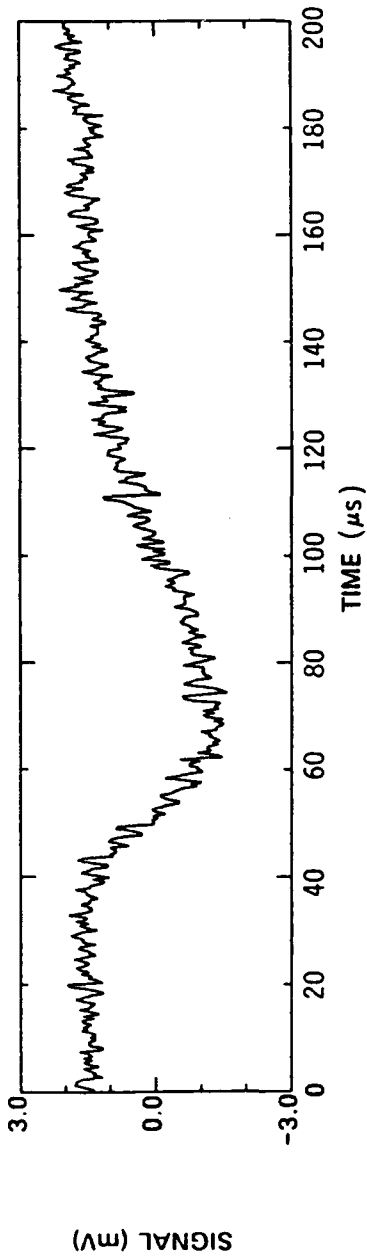
FIGURE 3-6b. 0.5 MHz SILICON APD NOISE RESULTS

PDH_ROST
24-MAY-91 11:16:54

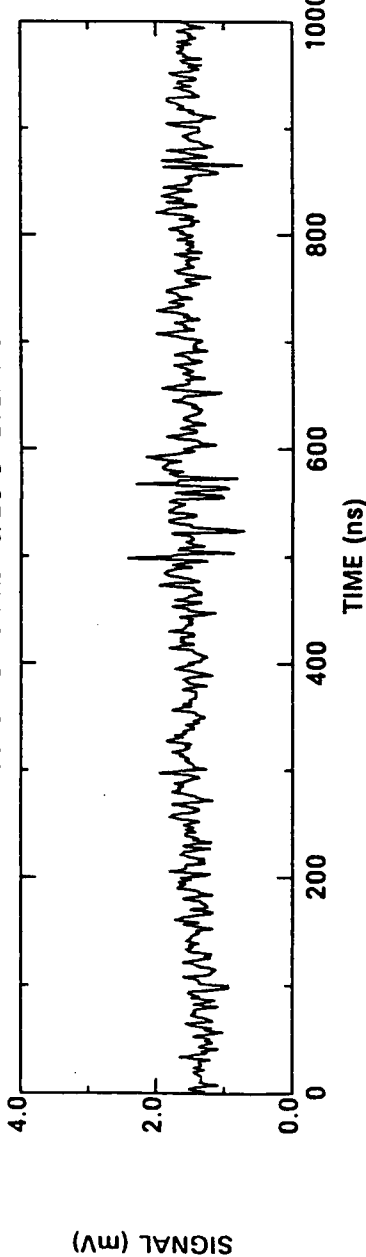
8616-PC 10 KHz 5/20 C EVENT 7



8616-PC 10 KHz 5/20 C EVENT 8



8616-PC 10 KHz 5/20 C EVENT 9



PDH_ROST
21-MAY-91 15:28:35

FIGURE 3-7a. 10 KHz SILICON PIN DIODE NOISE RESULTS

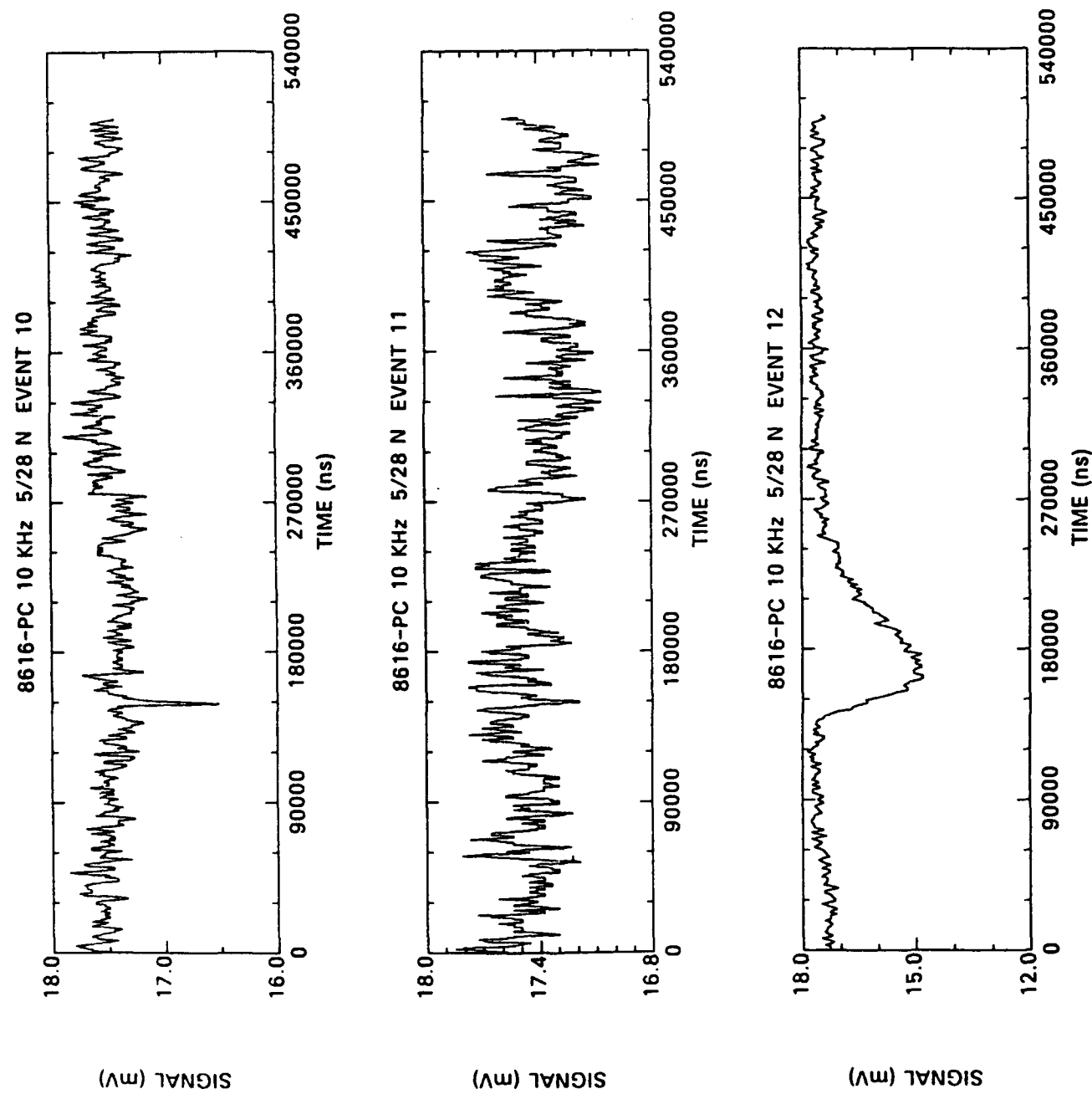
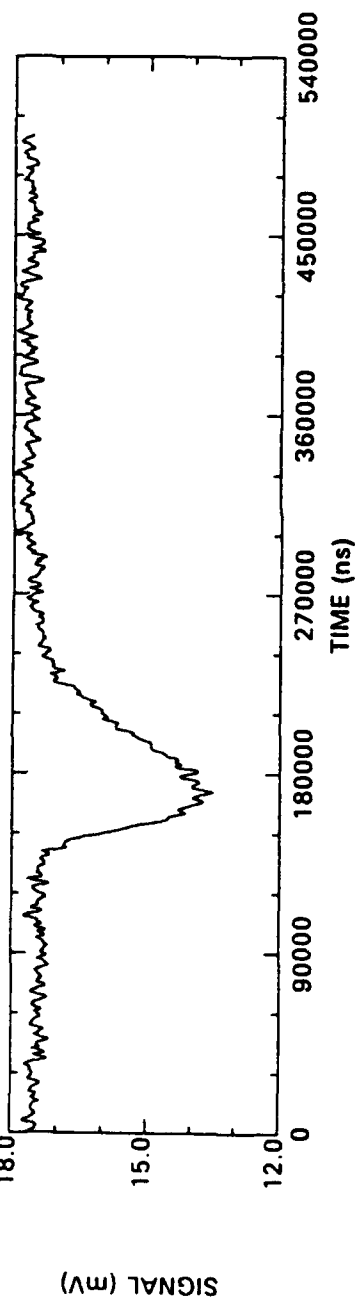


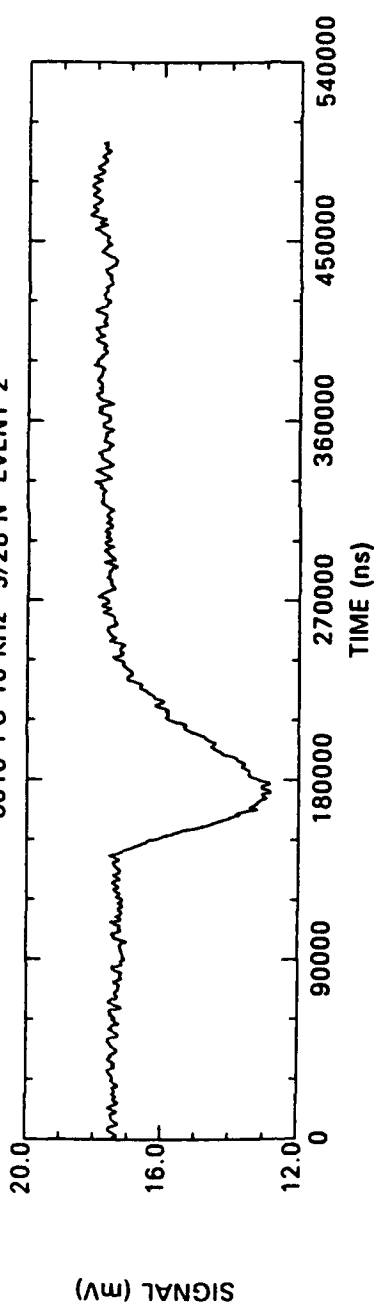
FIGURE 3-7b. 10 KHz SILICON PIN DIODE NOISE RESULTS

PDH_ROST
29-MAY-91 14:05:01

8616-PC 10 KHz 5/28 N EVENT 1



8616-PC 10 KHz 5/28 N EVENT 2



8616-PC 10 KHz 5/28 N EVENT 3

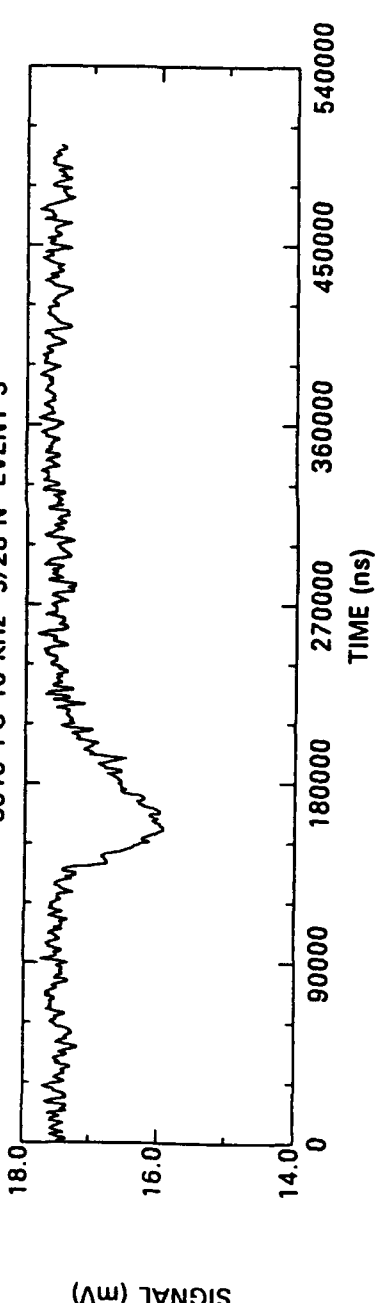
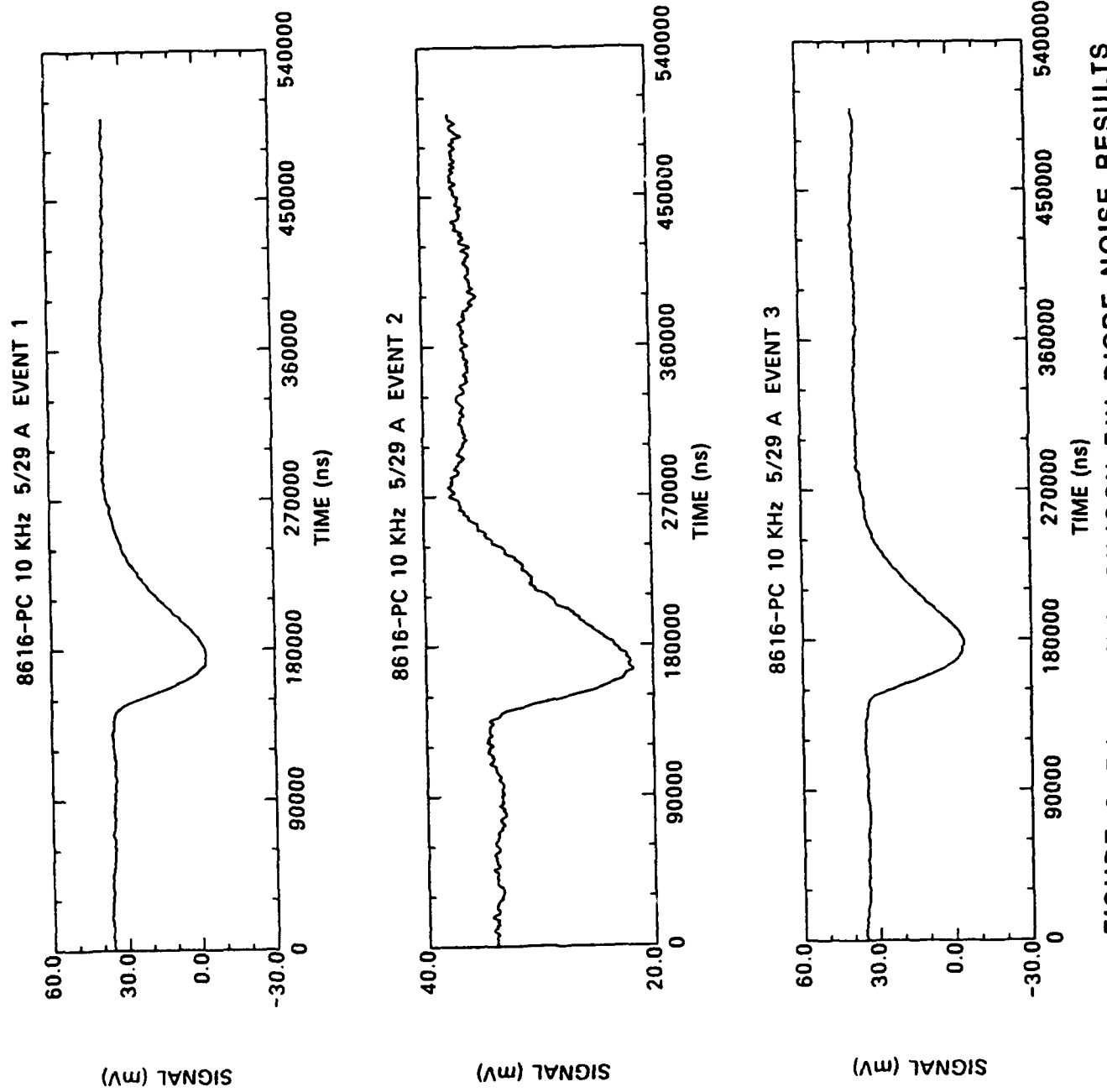


FIGURE 3-7c. 10 KHz SILICON PIN DIODE NOISE RESULTS
PDH_ROST
29-MAY-91 14:01:52



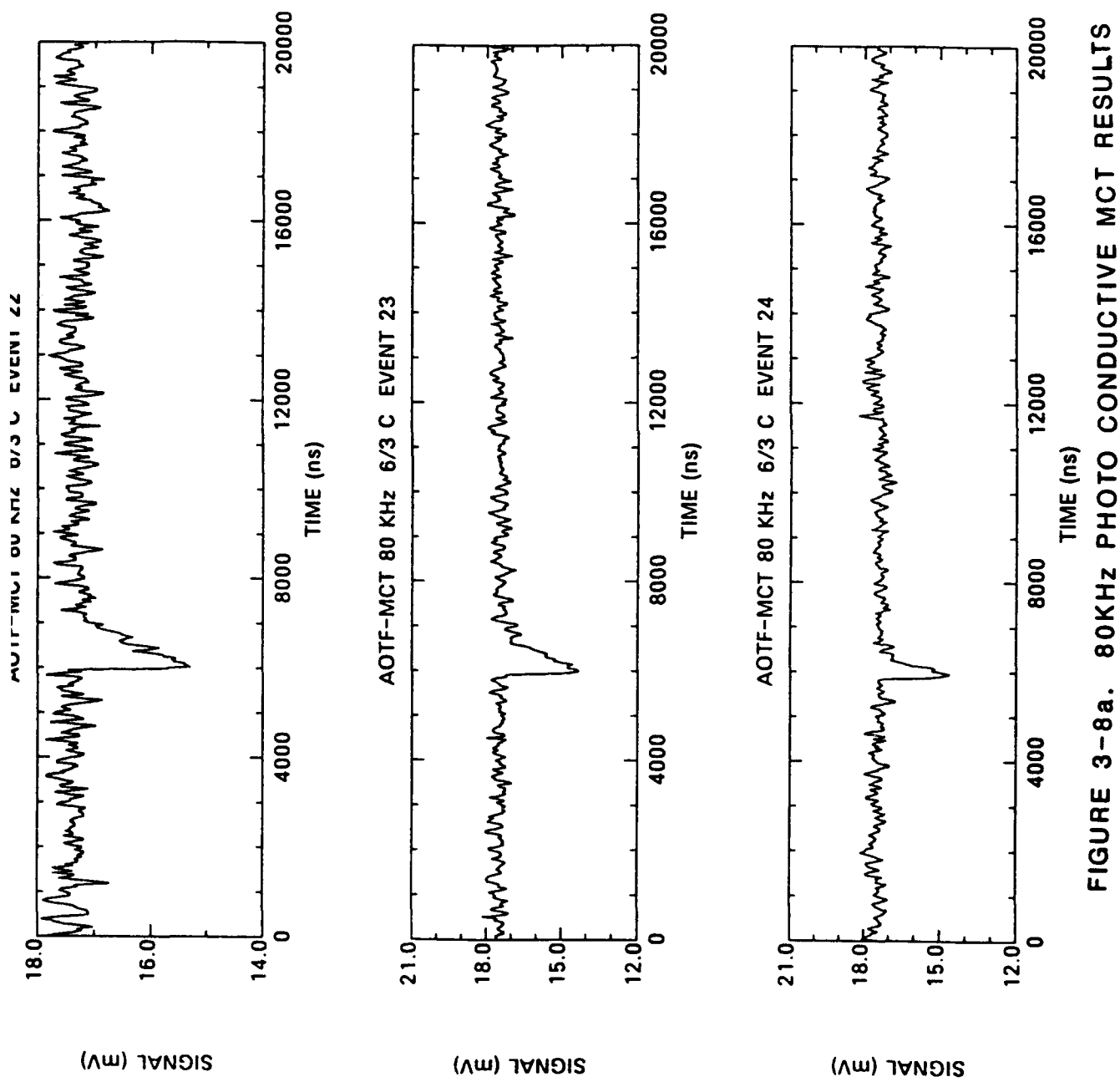


FIGURE 3-8a. 80KHz PHOTO CONDUCTIVE MCT RESULTS

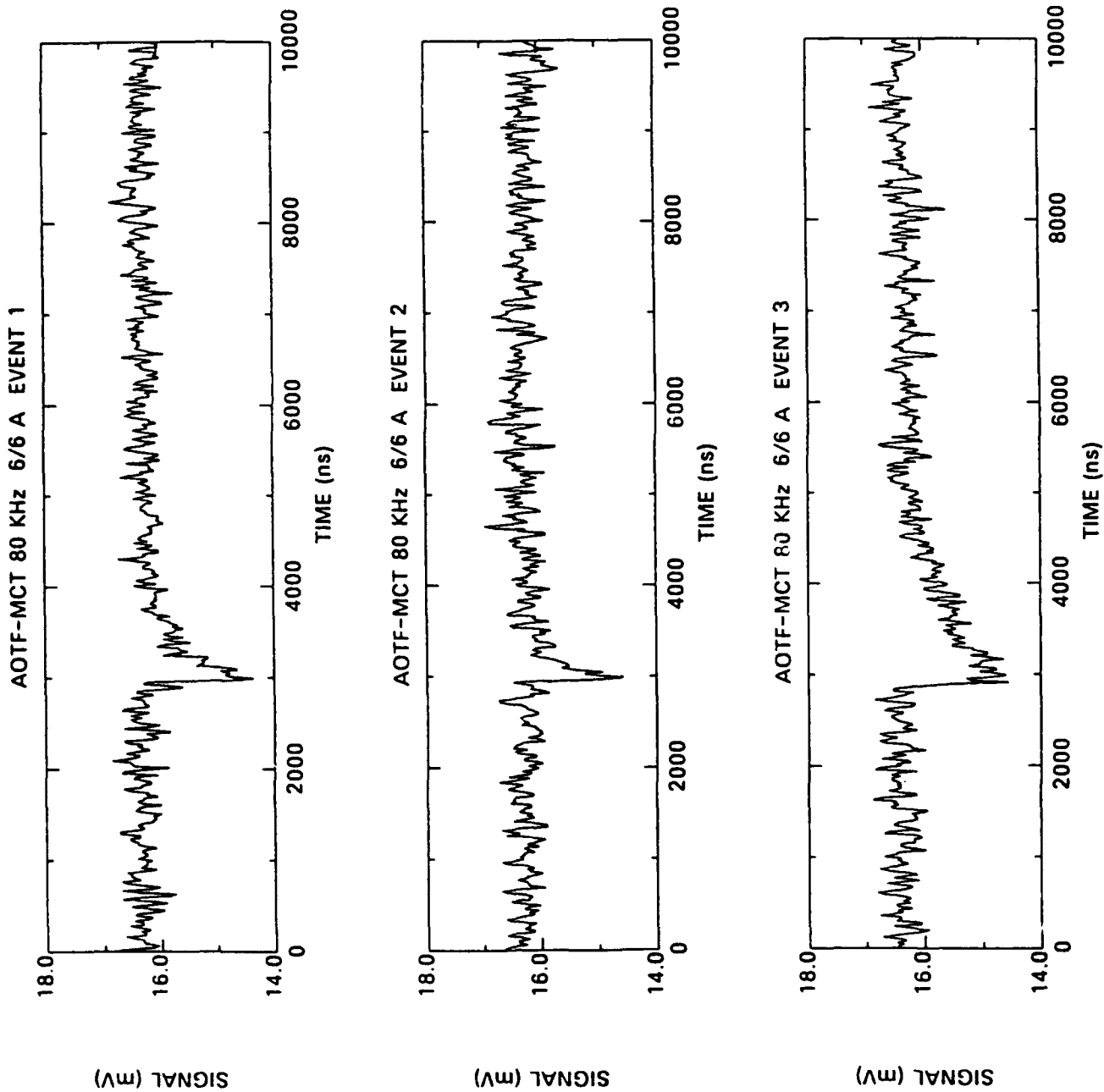
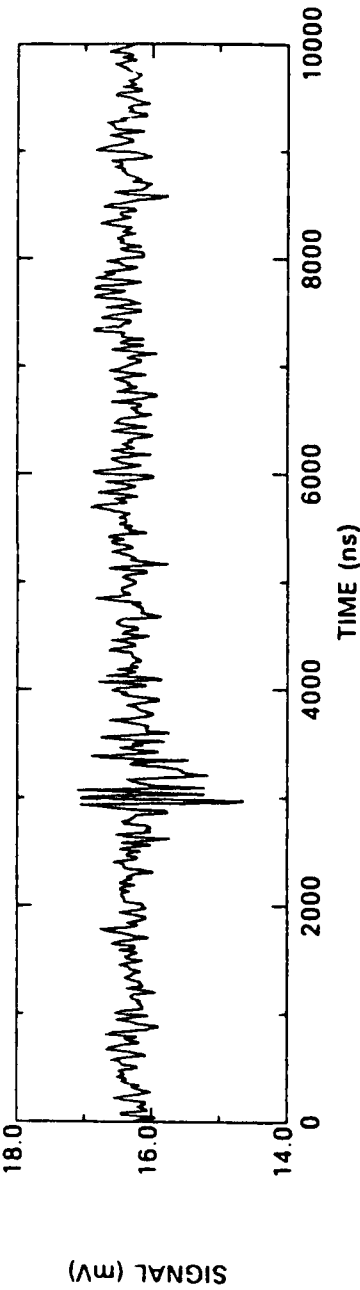


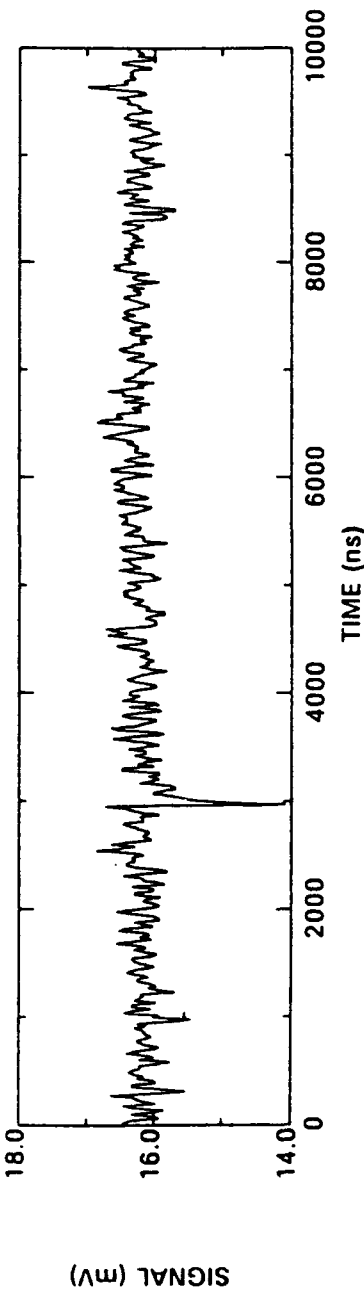
FIGURE 3-8b. 80KHz PHOTO CONDUCTIVE MCT RESULTS

PDH_R0ST
6-JUN-91 16:12:06

AO, F-MCT 80 KHz 6/6 A EVENT 25



AOTF-MCT 80 KHz 6/6 A EVENT 26



AOTF-MCT 80 KHz 6/6 A EVENT 27

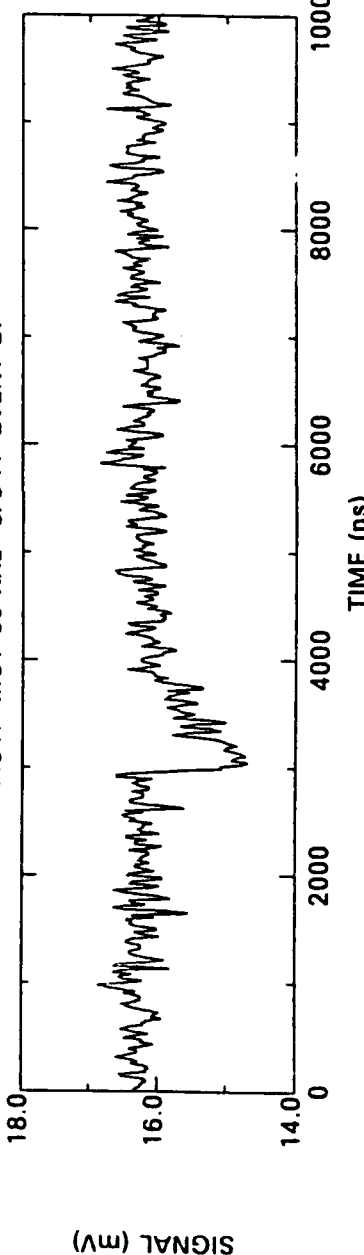


FIGURE 3-8c. 80KHz PHOTO CONDUCTIVE MCT RESULTS
POH_ROST
6-JUN-91 16:19:56

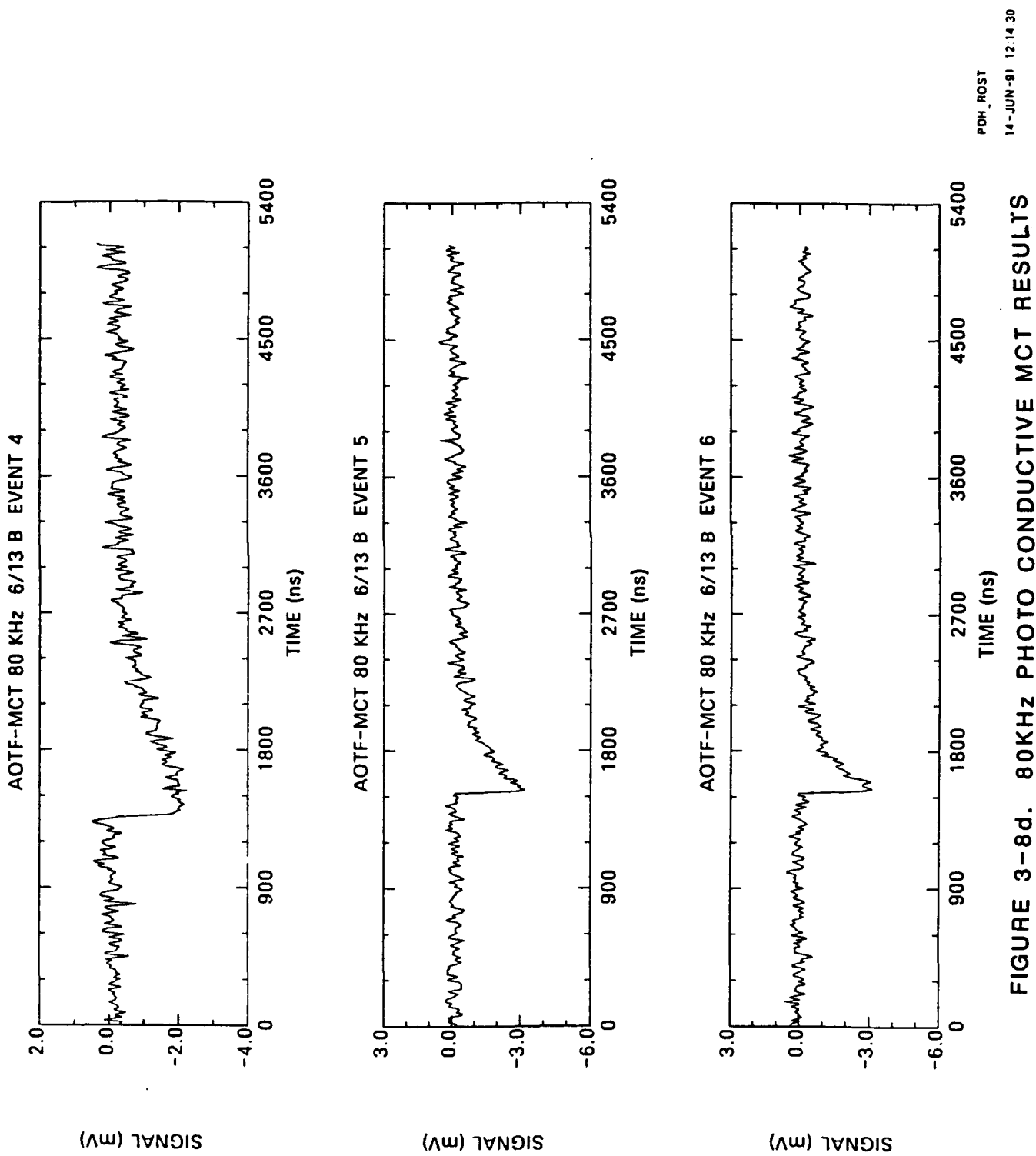


FIGURE 3-8d. 80KHz PHOTO CONDUCTIVE MCT RESULTS

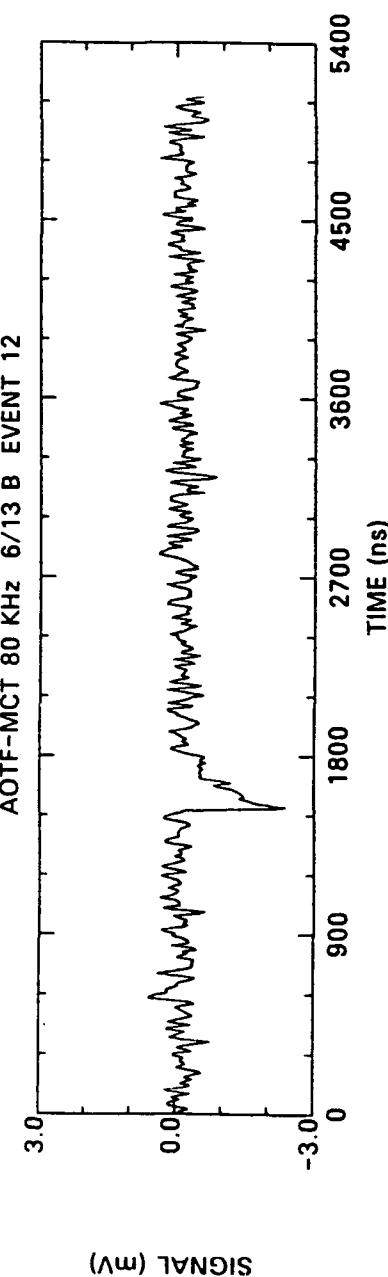
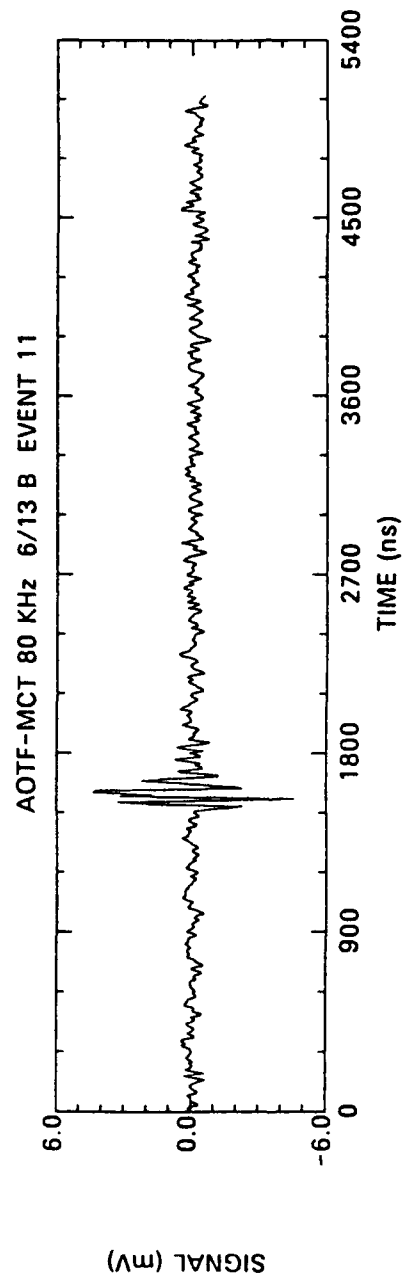
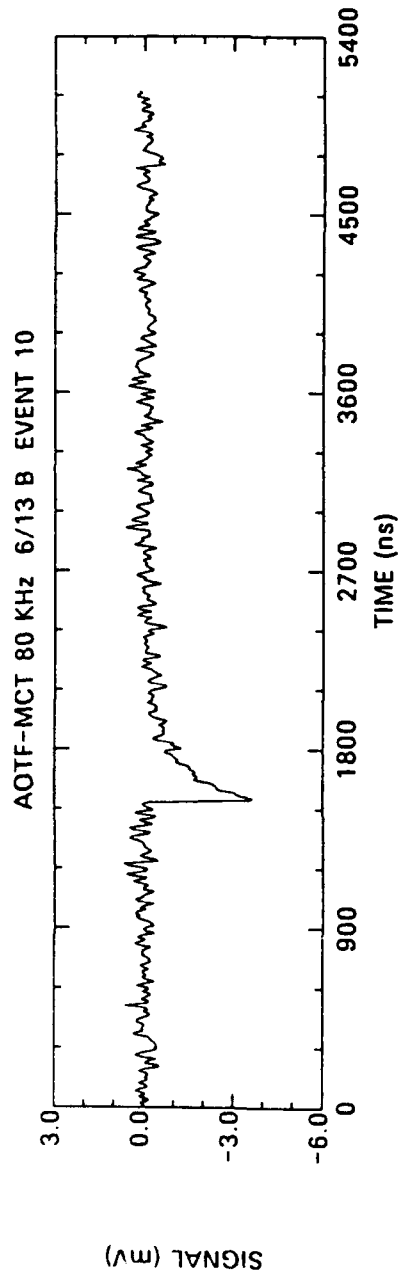


FIGURE 3-8e. 80KHz PHOTO CONDUCTIVE MCT RESULTS

14-JUN-91 12:15:14
EINH_ROST

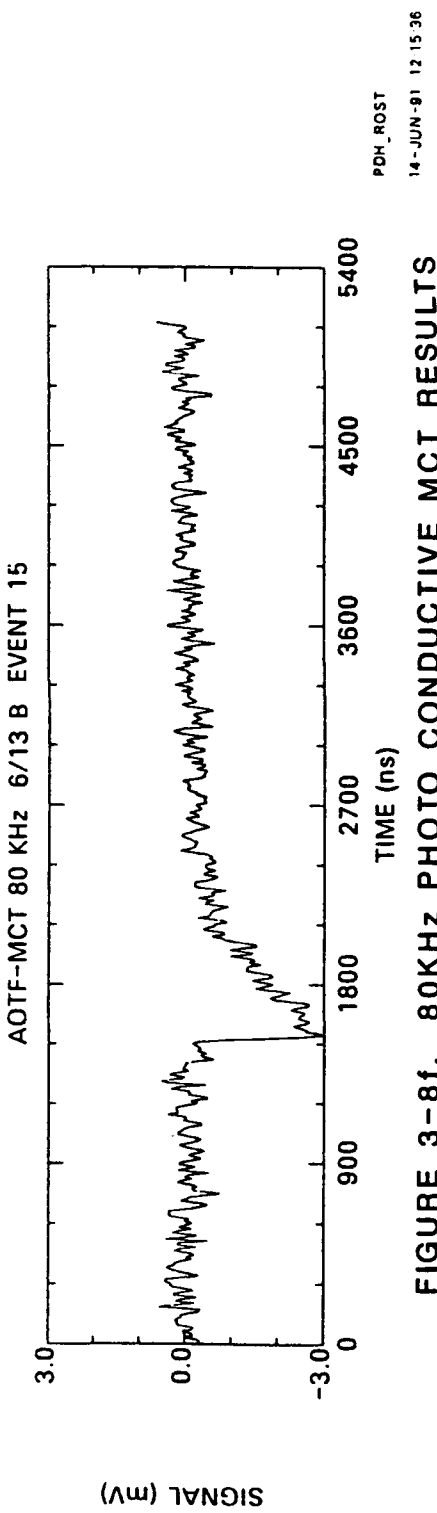
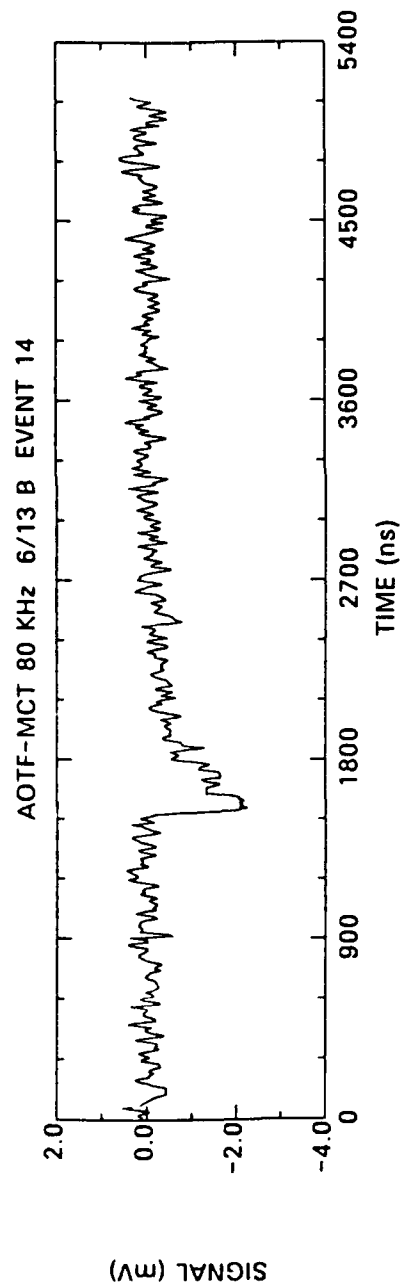
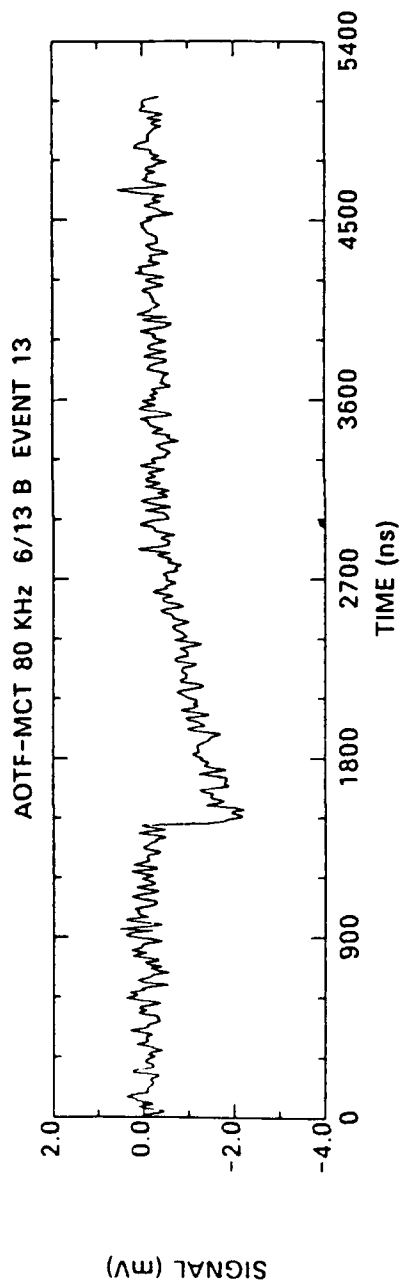


FIGURE 3-8f. 80KHz PHOTO CONDUCTIVE MCT RESULTS

TABLE 3-3. Detector Hit Rates

Unit	Detector Material	Case	Events	Time (Hr)	Rate (1/Hr)	Area (cm ²)	Rate (1/Hr/cm ²)
8616-PC 10K	Silicon	5/20	2	0.848	2.4	0.887	2.7 9.4 17.4
		5/28	151	18.196	8.3		
		5/29	78	5.056	15.4		
DIA-APD 20M	Silicon	5/17-20	100	3.220	31.1	0.071	438
		5/21	35	1.097	31.9		449
DIA-APD 500K	Silicon	5/21-24	434	13.645	31.8		447
NERC-MCT	MCT	5/15-17	39	17.574	2.2	6.25E-4	3551.
AOTF-MCT	MCT	6/3	36	5.380	6.7	0.0314	213. 470. 780.
		6/13-18	164	11.113	14.8		
		6/5-6	174	7.107	24.5		

investigated. One possibility is that the higher rate is simply an artifact of the detector chip design. As a standard product, NERC fabricates detector chips with nine detectors of different sizes and shapes. Which detector is wired in the dewar is user selectable. It may be the case that the detectors all have a common anode and cosmic rays from any of them effects all of their electrical outputs. Not only would this be an important conclusion for interpreting experimental results, it would have a significant impact on future RL sensor designs. For example, if a common anode linear array were used in the actual sensor, there would need to be special cosmic ray trapping logic built in. An experiment monitoring two detector outputs simultaneously should resolve this question. On the other hand, if the MCT-PV detector is more sensitive to cosmic rays than silicon, than this is crucial data to acquire before constructing a deployable sensor. In either case, additional cosmic ray detection experiments are needed in a future effort. In addition, the cosmic ray tests need to be carried out with the MCT-PV detector and the three preamplifiers, once the noise problems have been resolved.

4. GAS CELL ABSORPTION EXPERIMENT

4.1 Theory and Objectives

The goal for the gas cell absorption experiment was to experimentally test the differential absorption of CO₂ laser radiation versus blackbody radiation through a CO₂ absorption cell. The CO₂ absorption cell concept is of interest for false alarm discrimination because of its simplicity and potential use in wide field of view applications. The concept is to split light from a common aperture into two beams and pass one beam through a non-absorbing cell while passing the other beam through the CO₂ absorption cell. Conceivably, a voltage ratio measurement could be made of these two channels to characterize the radiation source as being of laser origin or not. The capability for this technique to discriminate false alarms derives from the highly structured CO₂ absorption spectrum illustrated in Figure 4-1. CO₂ laser radiation is at a wavelength on the peak of the absorption curve for the CO₂ gas cell. Broadband radiation must be integrated over the CO₂ absorption lines and, therefore, has significantly less percentage absorption of the incident signal. Therefore, the signal ratios of the CO₂ cell to the non-absorbing cell should be significantly different for the two types of radiation sources.

Model predictions for the differential absorption effect were made with the FASCODE computer model in conjunction with a special utility code which integrated the FASCODE transmission file over particular source functions. The predictions indicate the considerable differential absorption is expected as the gas cell temperature is increased. This results from an increase with temperature in the population density of the CO₂ molecular energy levels which can absorb the CO₂ laser light. Increasing the CO₂ gas pressure degrades the differential absorption because the narrow CO₂ absorption lines become pressure-broadened, thereby increasing their absorption of broadband radiation.

4.2 Experimental Approach

The experimental set-up depicted in Figure 4-2 was constructed at SciTec to test the differential absorption technique. Chopped blackbody and laser radiation sources were used to illuminate the gas cell. The gas cell was evacuated to roughly 10⁻³ torr and filled with CO₂ at atmospheric pressure. CO₂ was bled to a water tank used to maintain a constant gas pressure in the cell. Radiant intensity was measured with a photoconductive MCT detector with a cooled long pass (9-12 microns) spectral filter. The filter was used to limit the detector's bandpass so as to avoid having the strong 4-5 micron CO₂ absorption lines interfere with the broadband transmission measurements.

4.3 Measurement Results and Conclusions

Table 4-1 presents a summary of the predicted and measured experimental results for the gas cell absorption experiment. The temperature trend predicted by FASCODE is clearly evident and the CO₂ laser absorption value agrees quite well with the prediction. However, the broadband radiation transmission through the elevated temperature cell is significantly lower than predicted.

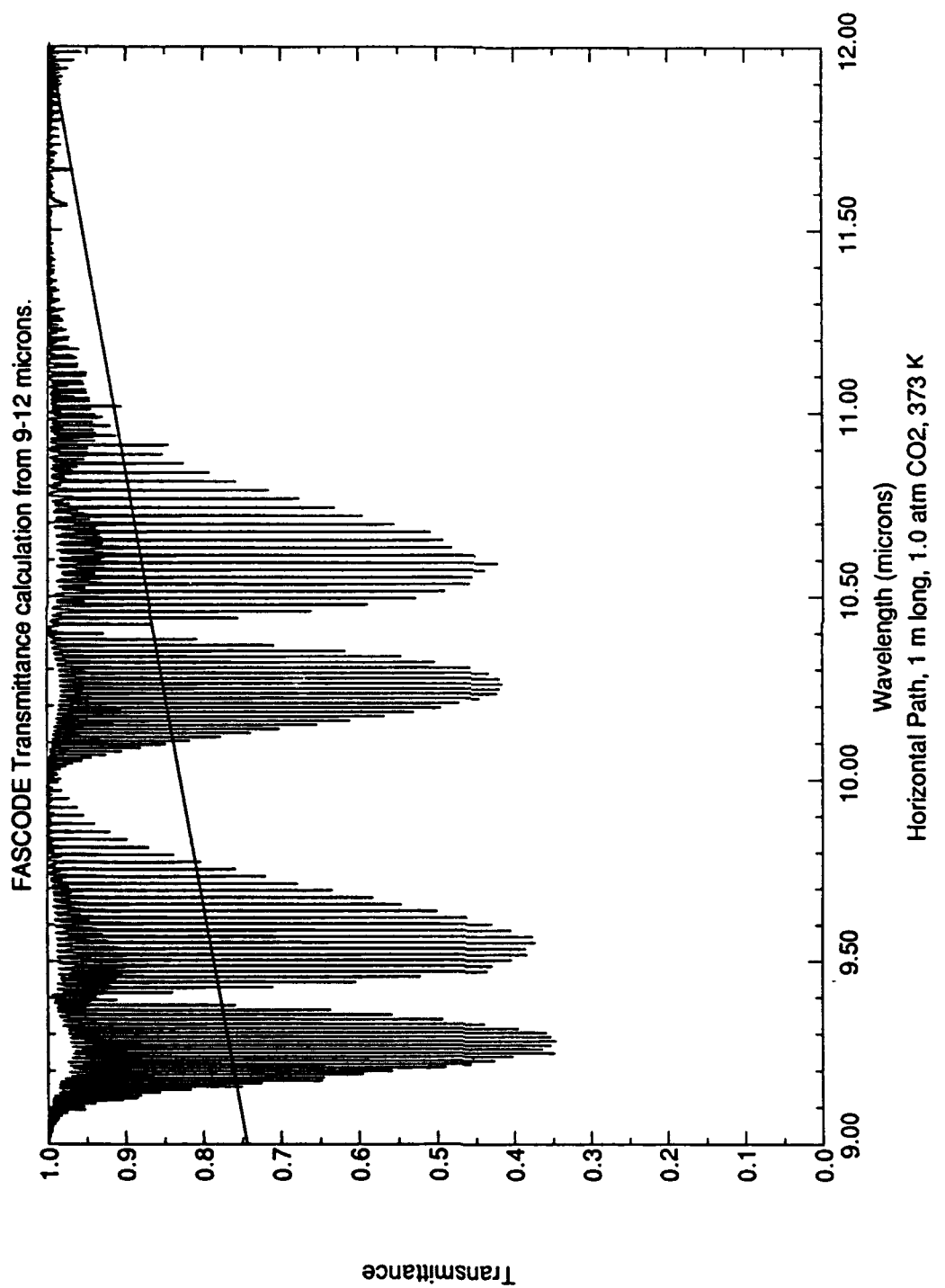


FIGURE 4-1. CO₂ Absorption Spectrum

QH
12-JUL-91 14 57:35

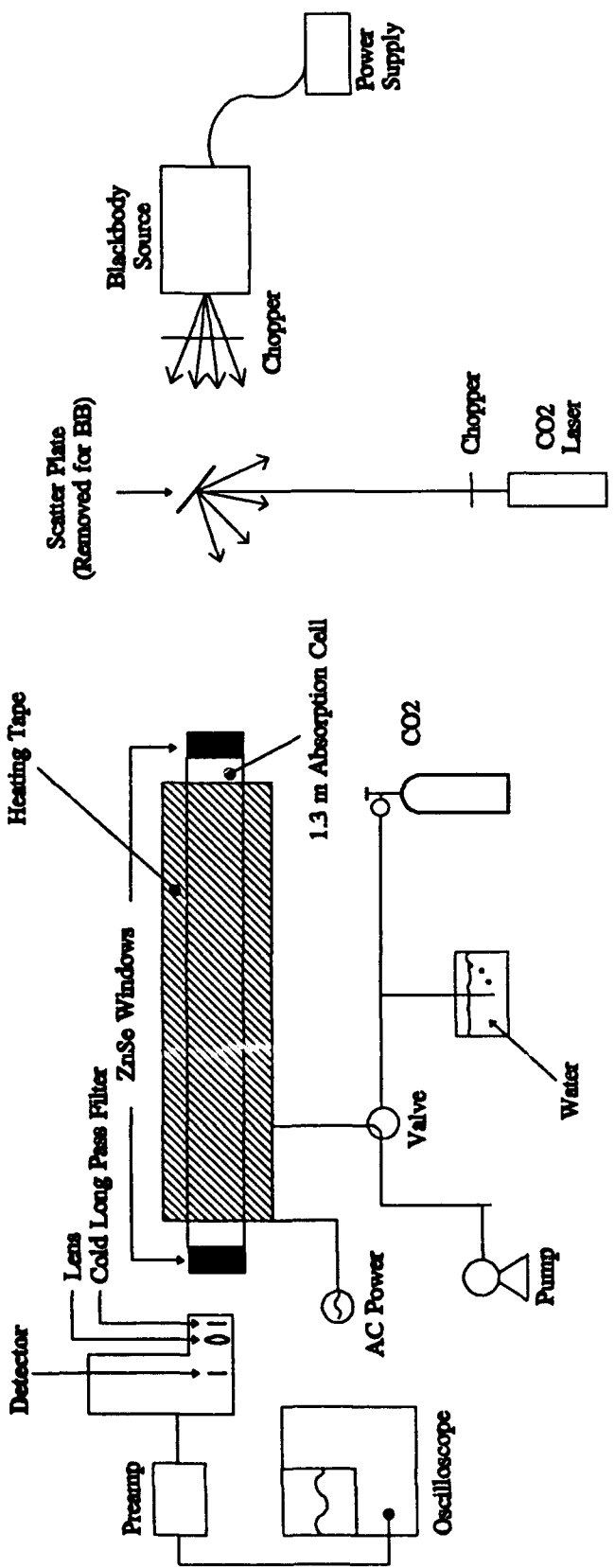


FIGURE 4-2. Experimental Set-up

**TABLE 4-1. Summary of the Predicted and Measured Experimental Results
for the Gas Cell Absorption Experiment**

Case	Gas Temperature	$T_{r_{BB}}$	$T_{r_{laser}}$	Absorption Ratio $\frac{T_{r_{laser}}}{T_{r_{BB}}}$
Prediction	25°C	0.99	0.92	0.93
Measurement	25°C	0.97	0.96	0.99
Prediction	100°C	0.95	0.31	0.32
Measurement	100°C	0.57	0.35	0.61

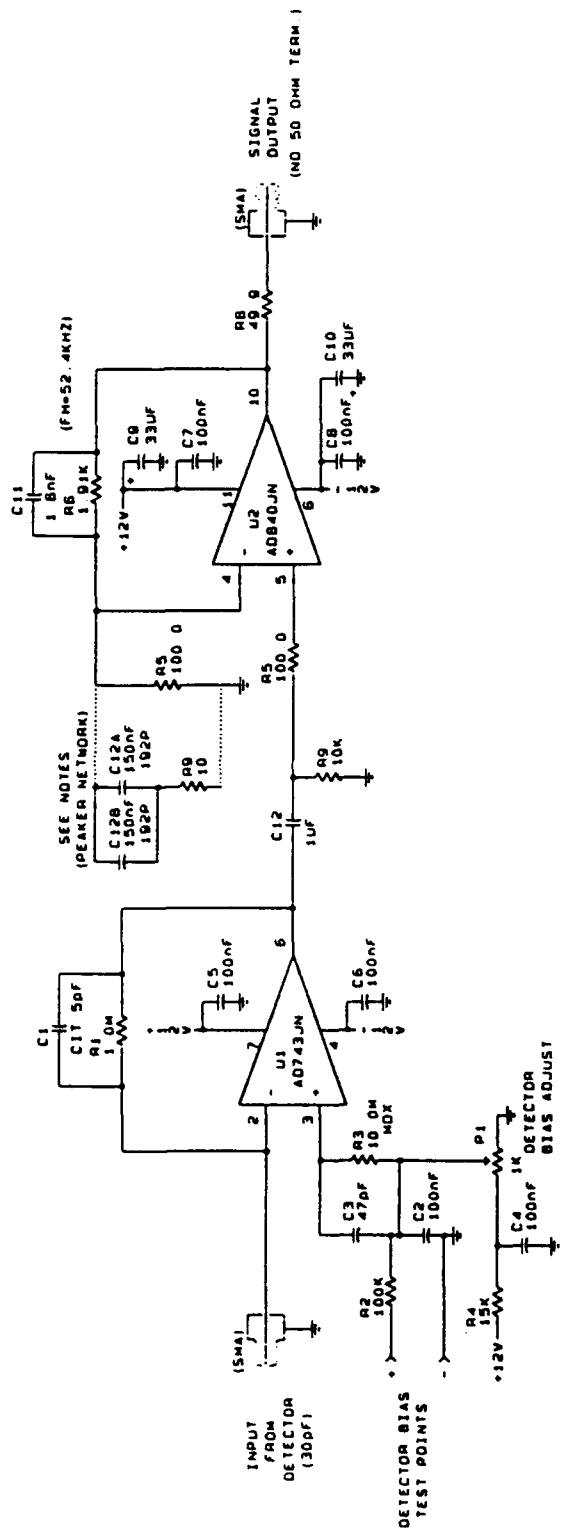
There are three possible explanations for this discrepancy. First, the FASCODE transmission predictions for the broadband radiation could be erroneous. This possibility seems remote and would require considerably more experimental evidence before a case could be made. Second, gas cell impurities, such as water, could have increased the broadband absorption while having little effect on the laser radiation. This possibility also seems remote as we kept a positive pressure of CO₂ in the cell to minimize any diffusion of impurities into the cell.

The third possibility is that the effect is an artifact of the experimental technique. Specifically, as the cell is heated, it emits more infrared energy. Some of this energy will hit the chopper blade and be reflected back to the detector. Since the blade is the cold part of the modulation (slot exposes hot blackbody), if more radiation reflects from the blade it will decrease the differential between the cold blade and the hot blackbody. This differential would be interpreted as a transmission loss since the detected signal's modulation depth would be less. For the laser transmission experiment, the chopper was in an off-axis location since a diffuse scatter target was used to create the laser signal. Thus, the radiation emitted by the cell would not find its way back to the detector through a reflection from the chopper blade. This explains how the laser transmission signal could agree with theory while the blackbody case didn't. We recommend that pulsed, broadband radiation sources be used in a future test to validate the broadband transmission predictions.

Despite the uncertainty in the broadband transmission results, the experiments show that differential absorption is a promising technique for optical false alarm rejection. Ideally, one would use both detectors in a coincidence approach so that if only one detector got a hit, the signal would be rejected as a cosmic ray. For this approach, the differential signal achieved with the 1.3 m path length is too large. Fortunately, it is desirable to shorten the tube anyway to save weight and space and increase the system's field of view. We recommend carrying out a design and breadboard of a CO₂ absorption cell differential radiometer for a particular mission. An optical design is needed to produce roughly a 0.7 attenuation factor for the laser channel. The required field of view will be derived from the scenario description.

APPENDIX

CIRCUIT SCHEMATICS



NOTES:

- APPROX 30KHZ 8M FOR 450F TOTAL INPUT CAPACITANCE
- FOR OPERATION FROM A 1200F DETECTOR
- 1330F TOTAL INPUT CAPACITANCE CHANGE
- C1 TO 1.5DF AND USE A HIGH PEAKER SECOND STAGE
- USE GROUND PLANE BOARD
- KEEP LEADS AS SHORT AS POSSIBLE
- BIAS POT ADJUST THRU WALL OF ENCLOSURE
- +/-12VDC SUPPLY. +/-30mA MIN RATING (+/-17mA NOM)

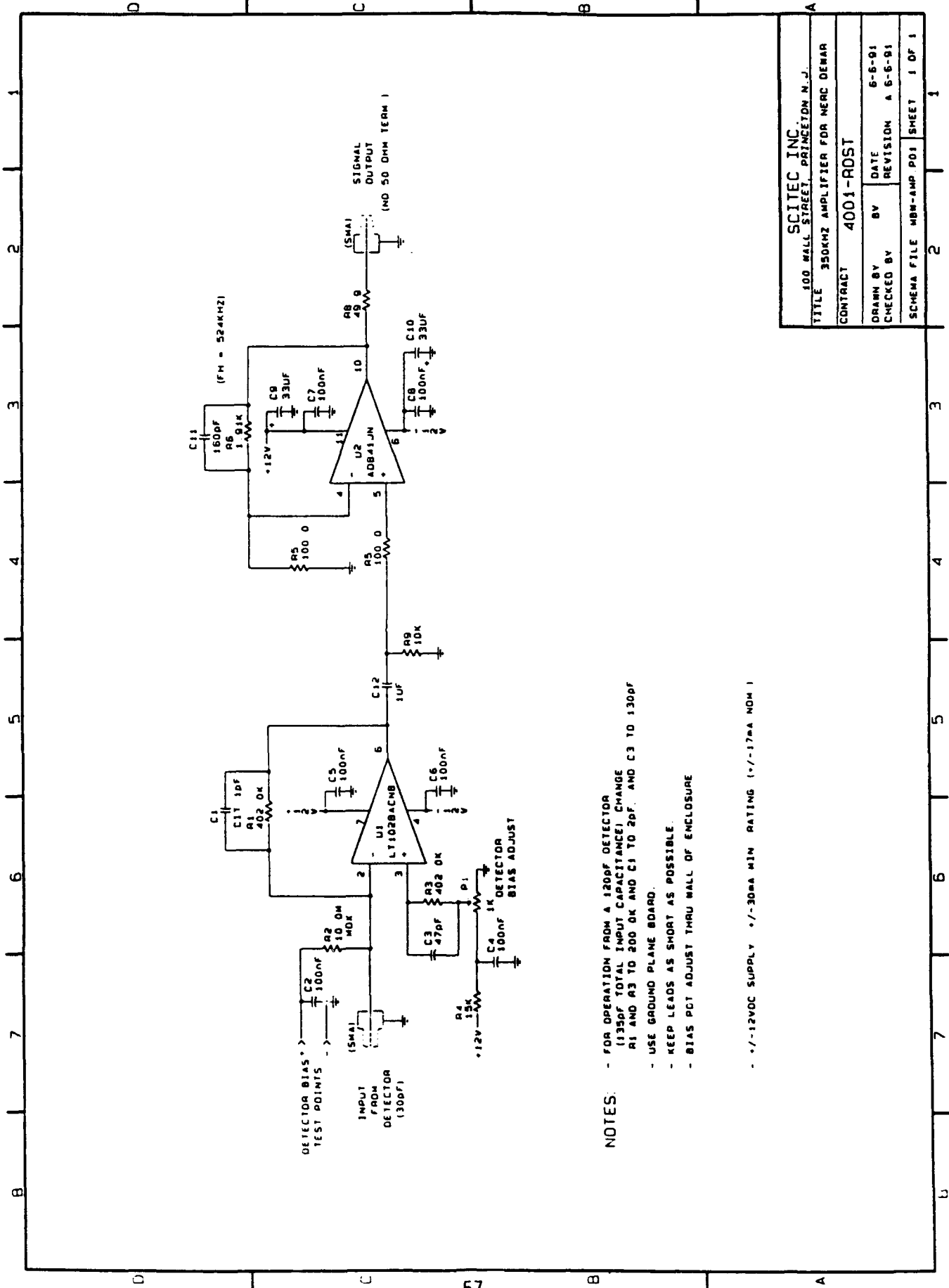
SCITEC INC.
100 WALL STREET, PRINCETON, N.J.
TITLE: 35KHZ AMPLIFIER FOR NERC DEMAR

CONTRACT: 4001-ROST

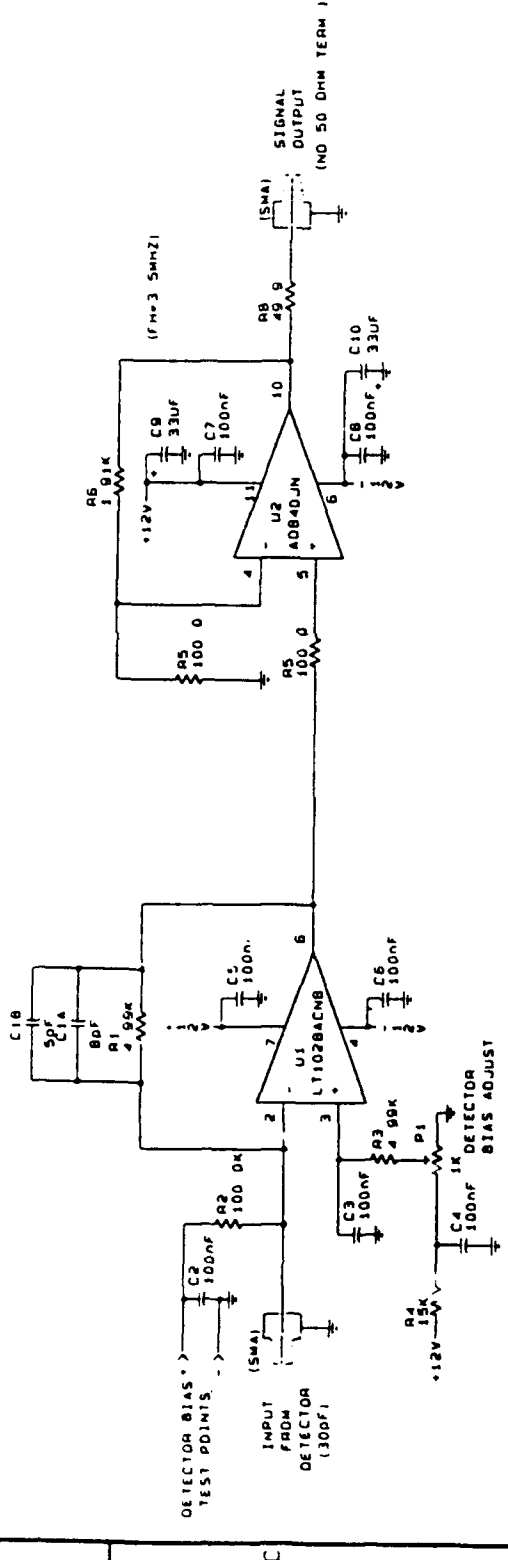
DRAWN BY	BV	DATE	6-6-91
CHECKED BY		REVISION	A

SCHEMATIC FILE: LBN-AMP.P01

SHEET: 1 OF 1



SCITEC INC.	A	
100 WALL STREET, PRINCETON N.J.		
TITLE	350kHz AMPLIFIER FOR NERC DEMAR	
CONTRACT	4001-ROST	
DRAWN BY	BV	DATE
CHECKED BY		REVISION
SCHEMATIC FILE MBIA-AMP P01 SHEET 1 OF 1		



NOTES.

- FOR OPERATION FROM A 120PF DETECTOR
 (1350F TOTAL INPUT CAPACITANCE) CHANGE
 R_1 AND R_3 TO 1.5K AND C_1 TO 27PF
- USE GROUND PLANE BOARD
- KEEP LEADS AS SHORT AS POSSIBLE
- BIAS POT ADJUST THRU MALL OF ENCLOSURE
- +/-12VDC SUPPLY. +/-30mA MIN. RATING (+/-17mA NOM)

SCITEC INC.	
100 WALL STREET, PRINCETON N.J.	
TITLE 3 5MHz AMPLIFIER FOR MECO DEMAR	
CONTRACT 4001-ROST	
DRAWN BY CHECKED BY	BV
	DATE REVISION
	6-6-91 A
SCHEMATIC FILE	MBB-AND P01
SH/ET	1 OF 1

REFERENCES

- (1) RL Laser Sensor Study Final Report (Document No. 1482-1321S) for Contract Number F30602-89-C-0110
- (2) CW Radiometry Program, Final Report for WL, Contract Number F33615-86-C-1040, November 1989
- (3) Dereniak, Eustace L., Optical Radiation Detectors, John Wiley & Sons, Inc., 1984